Drones' Tactile Navigation using Biomimetic Vibrissal Sensors

Thesis Report

Mahima Yoganarasimhan

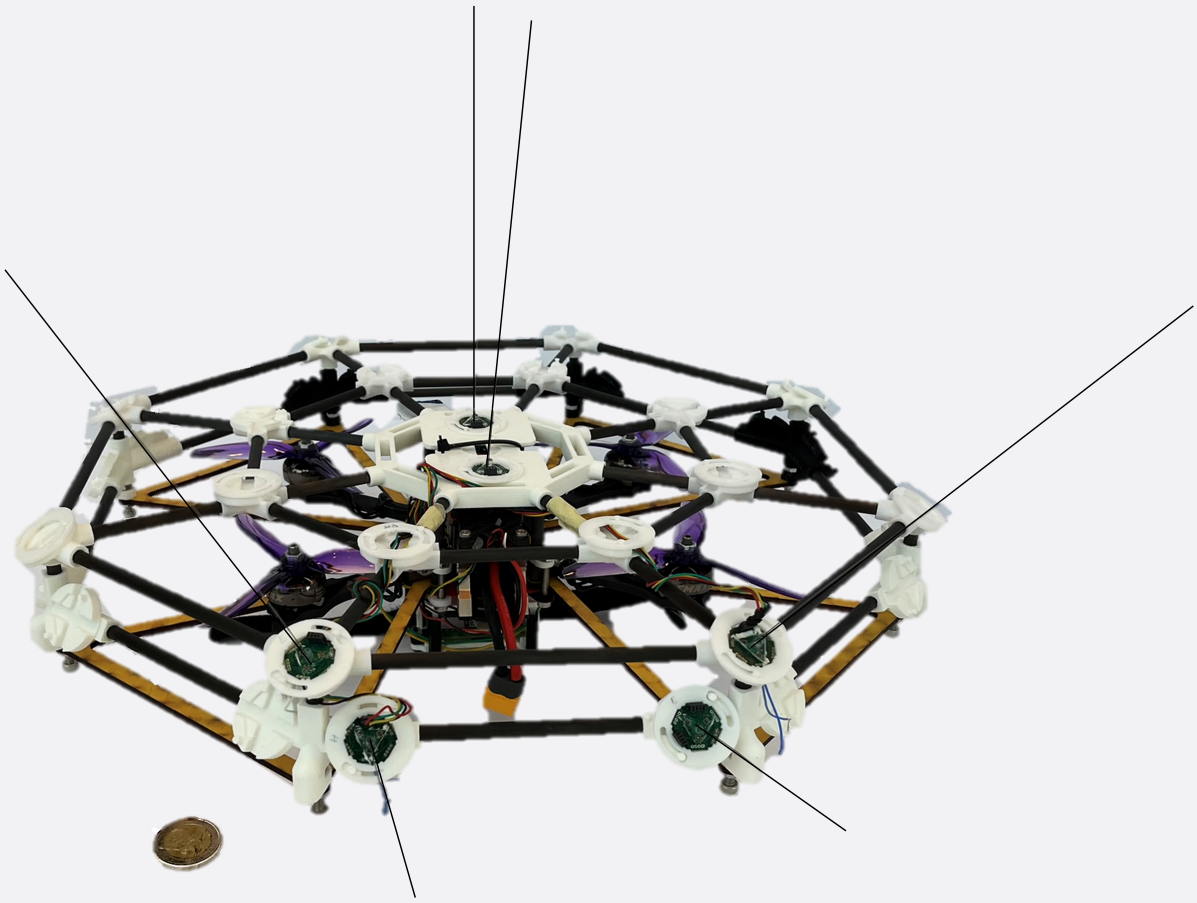

TU Delft

[This page is intentionally left blank]

Drones' Tactile Navigation using Biomimetic Vibrissal Sensors

Thesis Report

by

Mahima Yoganarasimhan

to obtain the degree of Master of Science
at the Delft University of Technology
to be defended publicly on September 11, 2024 at 09:30

Thesis committee:

Chair:	Prof Dr. G.C.H.E De Croon
Supervisor:	Dr. S. Hamaza
External examiner:	Dr. K. Masania
Place:	Faculty of Aerospace Engineering, Delft
Project Duration:	October, 2023 - July, 2024
Student number:	4670019

An electronic version of this thesis is available at `http://repository.tudelft.nl/`.

Faculty of Aerospace Engineering · Delft University of Technology

Preface

This thesis marks the culmination of my Masters journey at the Faculty of Aerospace Engineering, Delft University of Technology. The research presented here explores the tactile navigation of drones using biomimetic vibrissal sensors, a field that merges biology-inspired engineering with advanced robotics. The specialized sensory organs of animals, particularly the whiskers of rodents and other mammals, serve as a testament to natures ingenious solutions for navigating complex environments. My goal has been to bring some of these biological insights into the realm of aerial robotics, where tactile sensing is relatively unexplored.

This project has been both challenging and rewarding, requiring a deep dive into areas as diverse as sensor design, signal processing, and real-time system integration. Coming into this thesis with no hardware experience, I was thrown into the deep end of robotics and everything that comes with it. The journey has been a learning experience, filled with moments of both frustration and excitement as ideas were brought to life. A special thank you goes to everyone at the MAVLab. The collaborative spirit at MAVLab is one-of-a-kind, and I already miss it.

I am especially grateful to my supervisor, Dr. Salua Hamaza, for her unwavering guidance, support, and encouragement throughout this journey. To Nils de Krom, without whom our drone might never have taken flight, thank you for being a friend and partner during our theses.

Im incredibly grateful to my family for always believing in me and giving me the motivation to keep going.

I hope this thesis will contribute to the ongoing research in biomimetic sensors and inspire further exploration in the field of aerial tactile navigation.

Mahima Yoganarasimhan
Delft, August 2024

Contents

Part I

Introduction

[This page is intentionally left blank]

Introduction

The rapid advancements in robotic technology have necessitated the development of sophisticated sensory systems, enabling robots to interact with their environment with greater precision and intelligence. Among various sensory modalities, tactile sensing plays a pivotal role in robotic perception, allowing robots to detect objects, navigate complex terrains, and perform precise manipulations. One promising approach to enhancing tactile sensing in robotics is the use of biomimetic vibrissal sensors, inspired by the specialized sensory organs of mammals such as rodents, seals, and cats. These whiskers provide exquisite sensitivity to tactile stimuli, enabling animals to perceive their environment with remarkable accuracy.

In recent years, research has focused on replicating the function and structure of natural whiskers to develop advanced tactile sensors for robotic applications. These biomimetic sensors offer several advantages over traditional tactile sensors, including lower weight, reduced power consumption, and the ability to function in diverse environmental conditions without altering the environment. This thesis explores the integration of biomimetic vibrissal sensors into aerial platforms, a relatively uncharted territory in tactile sensing. By leveraging the tactile capabilities of these sensors, this research aims to enhance the navigation and interaction capabilities of drones in complex environments. Hence, this thesis aims to answer the following research question and sub-questions:

"To what extent can a drone equipped with our modular whisker-inspired sensors achieve accurate contour following, measured by its ability to maintain a desired distance from contours?"

A **Metric Definition:**

- i How can accuracy in contour following be precisely defined in the context of maintaining a desired distance from a contour?

B **Methodology:**

- i How does the drone's performance vary when following contours with different curvatures?
- ii What are the key indicators of successful contour following, including wall contact identification, orientation inference, sustained contact, and consistent distance maintenance?

C **Literature Comparison:**

- i How does the performance of the sensor-equipped drone compare to the simple implementation by Jung & Zelinsky (1996) [1]?
- ii How does the performance of our drone solution compare to the complex contour-following solutions presented by Zhang et al. (2022) [2] and Xiao et al. (2022) [3], considering factors such as accuracy and robustness?

D **Challenges and Solutions:**

- i What are the primary challenges associated with mounting whisker-inspired sensors onto an MAV, considering factors such as vibrations, inertial effects, and interaction with the propeller wake?
- ii How can these challenges be addressed to ensure accurate and reliable contour following in a real-world environment?

E **Applications:**

- i What specific advantages does accurate contour following by the drone offer for search and rescue missions in environments with limited visibility, such as dark or smoke-filled areas?
- ii How could the drone's contour-following capabilities be applied to navigate and explore confined spaces, such as caves, that are challenging for human access?

The structure of the report is as follows. Firstly, Part II presents the research that was carried out to answer the above-mentioned research questions. In Part III, an extensive literature review is provided on whisker-inspired perception in robotics. The appendices can be found in Part V.

[This page is intentionally left blank]

Part II

Scientific Article

[This page is intentionally left blank]

Drones' tactile navigation using biomimetic vibrissal sensors

Faculty of Aerospace Engineering, Delft University of Technology

ABSTRACT

This study explores the potential of biomimetic vibrissal sensors for tactile navigation in aerial robotics. Inspired by the sophisticated sensory system of rodents, we developed a non-intrusive, whisker-based tactile sensor system integrated into a drone platform. The system enables real-time detection and navigation through complex environments by emulating the tactile perception capabilities of natural whiskers. Our approach includes a novel platform design for easy sensor integration, a preprocessing solution to mitigate signal distortion as well as a simple static calibration set-up to estimate normal contact distances. The effectiveness of the system was validated through contour following tasks, where the whisker sensors provided feedback for precise navigation along surfaces with varying orientations. Results demonstrate that our system can estimate normal distances and wall orientations with sufficient accuracy, despite challenges such as lateral slip. This research highlights the potential of whisker-inspired sensors in enhancing the tactile sensing capabilities of aerial robots, offering significant advantages over traditional tactile sensors in terms of weight, power consumption, and operational flexibility in diverse environmental conditions.

1 INTRODUCTION

Tactile sensing is an essential component of a robot's ability to interact with its environment. It enables robots to detect and identify objects, navigate through complex environments, and manipulate objects with precision [1]. One domain of research that has garnered interest in recent years is the use of biomimetic vibrissal sensors for tactile perception in robotics. Whiskers are specialized sensory organs found in many mammals, including rodents, seals, and cats. These structures are used for a variety of purposes such as navigation, prey detection, and social communication.

The vibrissal system of rats has long been employed as a classic model in neuroscience for investigating the mechanisms of sensorimotor integration and active sensing [2, 3]. Whiskers, or vibrissae, are an essential part of many animals' sensory systems. These specialized hairs provide tactile information about the environment in which the animal explores. The bending of the whisker shaft is converted to a neural signal by mechanoreceptors situated in the follicle [4]. Mimicking this behaviour for applications in robotics is a challenging, but compelling, objective.

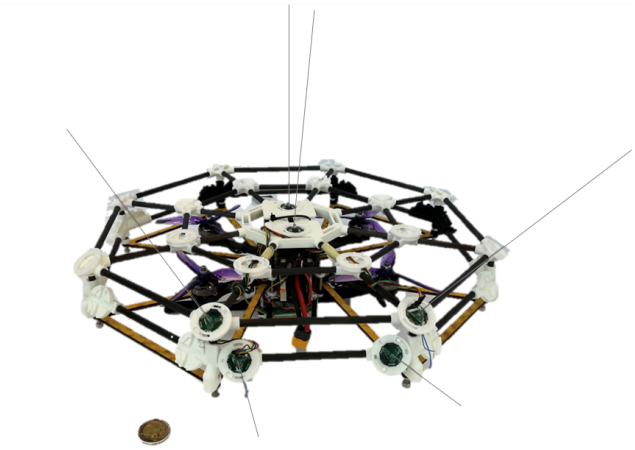

Figure 1 Our novel aerial drone platform for whisker integration. Size comparison with €2 coin.

Whisker-inspired sensors mimic the structure and function of natural whiskers and have several advantages over traditional tactile sensors. They are lightweight, low-power, and can operate in a wide range of environmental conditions. Literature demonstrates the potential to detect subtle changes in the environment, such as air currents [5–7] and texture gradients [8–10]. Arguably, one of the biggest advantages over traditional tactile sensors is that vibrissal sensors are non-intrusive, meaning that interaction with the environment does not require changing the state of said environment. Furthermore, unique environments such as smoke filled settings or covert operations in the dark may herald vibrissal sensing applications. These features make vibrissal sensing for tactile perception an intriguing sensory modality.

In our previous literature review [11], we categorized ongoing research into four distinct categories: shape inference, texture discrimination, fluid flow analysis, and navigation. Shape inference often depends heavily on a contact localization solution and is typically not resolved in real-time. Recently, Lin et al. [12] and Ye et al. [13] considered time-series information and data-driven solutions respectively that map whisker readings to distance estimations, which contrasts with the more common use of Euler-Bernoulli beam theory to model whisker behavior. In contrast, most navigation solutions do not address the contact localization problem directly and instead rely on occupancy maps [14, 15] based on binary touch events for exploration and robot localization.

Additionally, the majority of research has been conducted on robotic arms/end-effectors [12, 16–18], and ground-based mobile robots [15, 19–21]. To our knowledge, no research has integrated vibrissal sensing into aerial platforms until recently, when Ye et al. [13] proposed a biomorphic whisker sensor for aerial tactile applications. Therefore, this research focuses on developing an integrated navigation solution that uses real-time contact localization estimations as a controller input for an aerial platform. Our work will integrate the sensors proposed by Ye et al. [13] onto a novel aerial platform. The contributions of this study are listed below:

- We design and build a novel, modular drone platform that allows for whisker placement on top and around the side of the drone (Figure 1) .
- We propose a real-time preprocessing solution to combat the effects of vibration, hysteresis, and drift due to airflow on the whisker sensors.
- We propose a real-time contact localization solution using strategically placed whiskers and straightforward calibration. Our method achieves a root mean square error (RMSE) of 0.026 meters, with a standard deviation of 0.025 meters.
- We can determine the orientation of a surface with one contact event in real time, with an RMSE of 6.8°.
- We demonstrate setpoint tracking during contour following with a standard deviation of 0.041 meters using only the estimated normal distance as feedback.

2 Whisker Design and Manufacturing

We manufacture the whiskers as described by the method in [13]. The whisker consists of a 200mm nitinol wire shaft with diameter 0.4mm. The follicle structure is made up of a 5mm rubber tube, UV resin and three MEMS barometers attached to an integrated micro-controller PCB (see Figure 2A). The mass of the whisker is 1.52g.

The metal package covering the MEMS barometers is removed to expose the sensing element. The nitinol wire is straightened using a hot air gun at 520°C. A 2 mm thick stencil is placed on the PCB to create the triangular mold around the three barometers. A rubber tube, 5 mm in height with outer and inner diameters of 3 mm and 2 mm respectively, is positioned at the center of the three barometers. The PCB is then placed in a manufacturing/curing stand (see Figure 2B). The straightened nitinol wire is lowered into the rubber tube through a very small hole in the stand, ensuring it aligns perpendicular to the PCB surface. A syringe is used to inject 1.5 ml of UV resin into the rubber tube. The resin flows until a uniform surface is formed within the mold. The resin is cured under a UV lamp for two minutes, and for 48 hours in natural light after that.

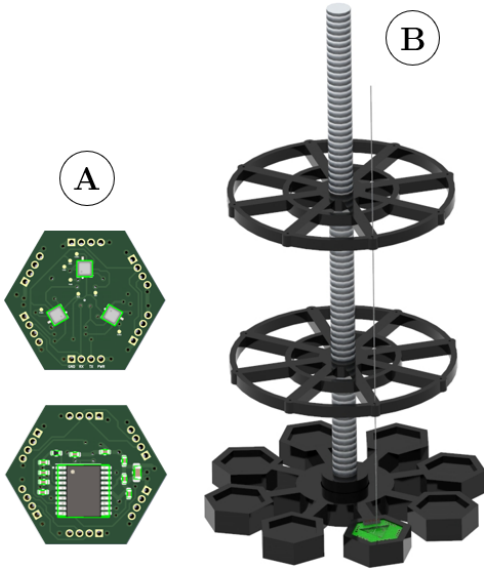

Figure 2 **—A:** Whisker base PCB with three integrated barometers (top) and STM32 micro-controllers (bottom) [13]. **—B:** Manufacturing and curing stand.

3 System Integration and Signal Conditioning

Frame	SpeedyBee FS225 V2 5 inch Frame
Electronic Speed Controller (ESC)	SpeedyBee F7 V3 BL32 50A 4-in-1 ESC
Autopilot	Pixracer R15 (PX4)
Companion Computer	Raspberry Pi 5 (Bookworm OS server)

Table 1 Components used on aerial platform

The barometers (BOSCH BMP390) are sampled at 50Hz through SPI communication by the STM32F070F6 (32Kbytes flash memory, 48 MHz CPU) microprocessor. The whiskers are integrated onto a novel aerial platform comprised of the components outlined in Table 1; they are serially connected to the Raspberry Pi 5 pinout and transmit data at 50Hz through UART. All signal reading, signal processing and navigation code is written in C++ and communication is achieved through ROS2. The Raspberry Pi is serially connected to the Pixracer autopilot, and communication between the two components is achieved through an XRCE-DDS bridge that converts uORB topics to ROS2 topics and vice-versa. ROS2 nodes and the DDS bridge run in their own respective docker containers with ROS2 humble base image to ensure modularity. A visual representation of the system architecture can be found in Appendix A.

To reduce the effects of temperature drift, the BMP390 register is accessed to apply the temperature compensation coefficients to raw data as specified by the manufacturer's manual. On the Raspberry Pi, additional preprocessing is

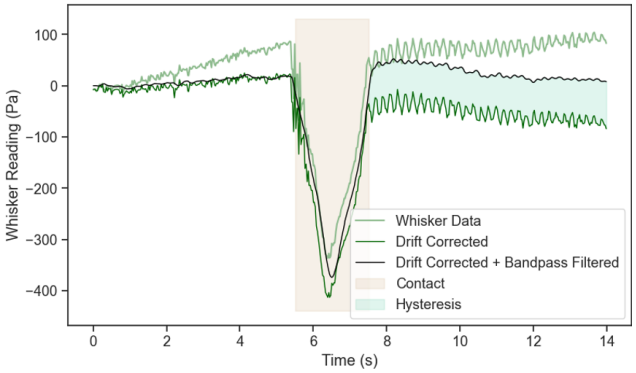

Figure 3 Preprocessing steps for incoming whisker data to mitigate effects of vibration, drift and hysteresis. Plots shown for one barometer during flight in which contact is made with a wall head on, and then moves back. The incoming data (light green) shows drift due to air pushed onto sensors during flight. This is corrected online by estimating the linear rate of change in pressure during an in-flight calibration sequence and correcting subsequent readings (dark green). Hysteresis is observed due to low frequency signals that arise from the soft materials during the unloading phase. The effect of signal noise and hysteresis is filtered out by means of a 1st order Butterworth bandpass filter (black).

done to combat the residual effects of platform vibration, hysteresis and drift. The resulting data is shown in Figure 3. The aggressive drift that is observed in the whisker data is caused by the air pushed onto the barometers by the propellers. This is compensated by identifying the rate of change of pressure in a calibration sequence performed in the first 35 seconds of flight. After takeoff, the drone holds its position for 20 seconds to allow the whiskers to return to their nominal state and for the nonlinear effects of takeoff-induced drift to stabilize. In the subsequent 15 seconds, the whisker data is recorded and a linear rate of change is computed. Using this, the successive whisker data is flattened to reduce the effect of drift. The effect of this drift compensation is shown by the dark green curve. Noteably, after the contact period, the pressure does not return to the nominal state. To account for this hysteresis and to reduce noise, a 1st order real-time Butterworth band-pass IIR filter with passband frequency of 0.03 to 3Hz is applied to the data. The drift-corrected and bandpassed data is used for contact detection and contour following in this study.

For the aerial platform, we propose a modular mechanical design (Figure 1) that allows whiskers to be easily placed at various designated points on the drone. This is achieved using 3D printed connector-clamping pairs arranged in an octagonal shape with carbon rods. The platform supports whisker placement either on top of or on the side of the quadcopter, making it suitable for multiple applications and enhancing its sensory capacity. A simplified render of the platform is shown in Figure 4. In this research, we place whiskers in the two front connectors for object detection and contour following. The connectors are angled upwards by 30° to ensure consistent behavior during binary contact events and sweeping motions, as further discussed in subsection 4.2.

4 Navigation

4.1 Environment and behaviour

We equip the aerial platform with two whisker sensors placed at the front of the drone, as shown in Figure 4. As previously mentioned, the whiskers are placed at a 30° angle. The drone's behaviour is controlled by a finite state machine (FSM) running at 50Hz, illustrated by Figure 5. The FSM comprises five states; calibration, waypoint navigation, surface evaluation, contour following, and land. The surface evaluation and contour following states make use of the preprocessed whisker data in real-time, and are further explained in Subsection 4.3.

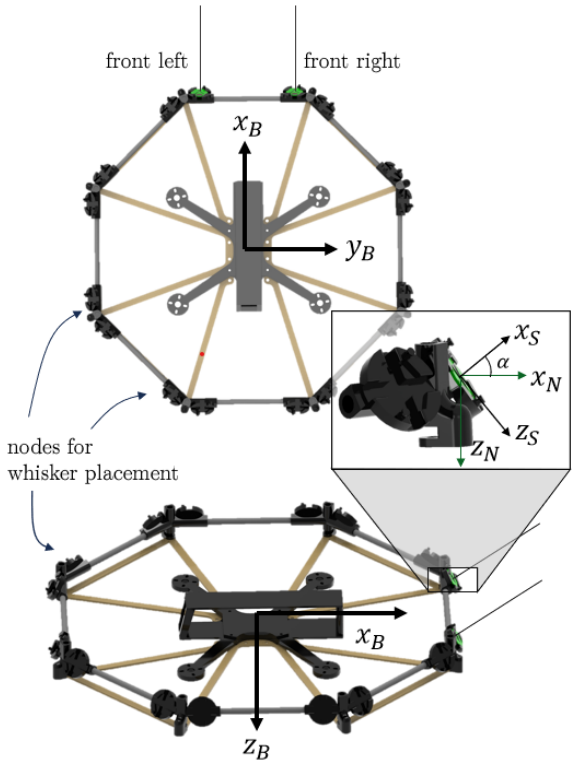

Figure 4 Simplified render of aerial platform. Top section removed to show nodes used for this study. We define three different reference frames. The drone body frame $\{\mathcal{B}\}$, the sensor frame $\{\mathcal{S}\}$, and the normal frame $\{N\}$. The $\{\mathcal{S}\}$ frame is aligned with the sensor, such that the x-axis always points along the undeflected whisker shaft. In this research, the whiskers are angled up by 30°($\alpha = 30°$).

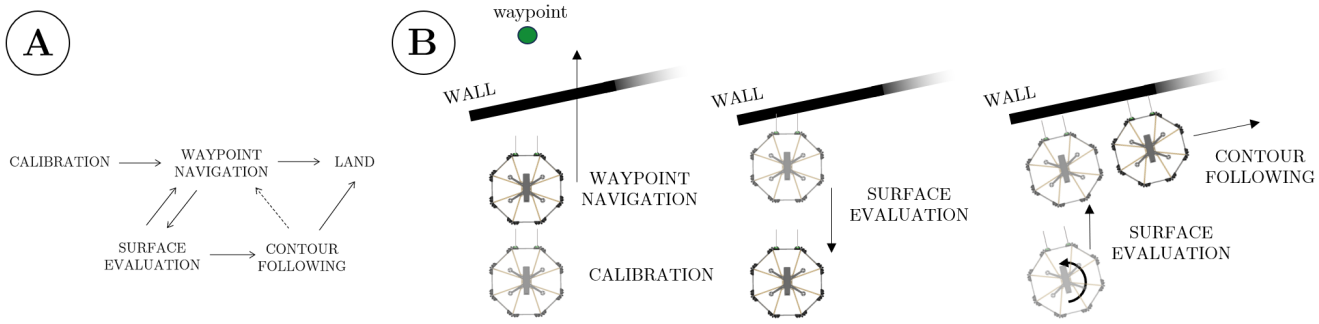

Figure 5 Finite State Machine (FSM) Logic. After takeoff, the drone initiates a calibration sequence to perform the preprocessing steps outlined in Section 3. It then transitions to the waypoint navigation state, where it travels to a predetermined waypoint. If the contact threshold of either whisker is exceeded, the drone reverses and enters the surface evaluation state. During this state, the surface orientation is estimated based on the contact event, and the drone is reoriented accordingly. It then returns to the initial point of contact. If contact is confirmed, the drone transitions to the contour following state, where a controller maintains a fixed distance to the surface as described in subsection 4.3. Once contour following is complete, the drone re-enters the waypoint navigation state. Upon reaching the waypoint, the drone initiates the landing state. To conserve battery and for simplicity, the drone will proceed to the land state immediately after completing contour following in this study.

Control of the drone is achieved by supplying trajectory set-points to the PX4 position controller in the world reference frame $\{\mathrm{W}\}$. We will denote world-frame coordinates $\{x, y, z\}^T$ as $\vec{\mathbf{p}}$. Let $\vec{\mathbf{p}}_i$ and $\vec{\mathbf{p}}_{wp}$ denote the current position of the drone and the waypoint respectively. A smooth trajectory is generated by sending incremental waypoints $\vec{\mathbf{p}}_{i+1}$ to the PX4 position controller of magnitude k, as in Equation 1. In this research k = 0.1 meters.

$$\vec{\mathbf{p}}_{i+1} = \vec{\mathbf{p}}_i + \frac{\vec{\mathbf{p}}_{wp} - \vec{\mathbf{p}}_i}{\left|\vec{\mathbf{p}}_{wp} - \vec{\mathbf{p}}_i\right|} \cdot \mathrm{k} \tag{1}$$

4.2 Contact localization method and assumptions

Generally speaking, contact locations along the whisker shaft and resulting whisker deflections are non-unique pairs. In literature, efforts have been made to accurately estimate contact location by means of Euler-Bernoulli beam theory [22], data driven methods [13], and time-series methods [12]. By leveraging smart positioning of the whiskers on the robotic platform, we reduce the expected state space of the whisker deflection. As a result, we use a simple linear regression to demonstrate sufficient accuracy for navigation tasks. As illustrated by Figure 4, three reference frames are defined. Let $\{\mathcal{S}\}$ denote the sensor frame, where the x-axis points in the direction of the whisker shaft. We can define reference frame $\{\mathrm{N}\}$ as the normal reference frame. We will describe the contact location in this reference frame. Listed below are the assumptions made:

1. Deflections of the whisker only occur about the sensor's local y-axis (deflections occur in the xz-plane). This will be true for whiskers positioned as shown in Figure 4 and for contact with objects of low curvature. We will limit our work to contact with flat walls.
2. The whisker does not buckle, it only bends. This implies no contact at the tip of the whisker, only along the shaft.
3. Friction on the whisker shaft has negligible effect on the sensor readings.

The sensitivity of the whisker in the expected deflection direction is determined through a simple static calibration setup. By mounting the whiskers at a 30° angle, bending primarily occurs around the y-axis of both the $\{\mathcal{S}\}$ and $\{N\}$ frame. In addition, for contour following we are only interested in the normal contact distance, reducing the problem to 1D contact localization. During static calibration, the whisker is set up identically to its placement on the platform: in an angled connector with barometer 3 aligned with the attachment point of the whisker to the base (See Figure 6). In this configuration, the bending stress at barometer 3 is solely due to the bending deflection around the local y-axis when contact is made.

Our calibration model $g : \mathbb{R} \to \mathbb{R}$ maps the whisker's pressure reading to a 1D contact location. If $\vec{\mathbf{p}}_{\mathcal{S}}$ and $\vec{\mathbf{p}}_N$ are the contact location $\{x, z\}$ in the sensor and normal frame respectively, then the rotation matrix ${}^{\mathcal{S}}\mathbf{R}_N$ between them is given by Equation 2 ($\alpha = 30°$).

$$\begin{bmatrix} x_N \\ z_N \end{bmatrix} = \begin{bmatrix} \cos\alpha & \sin\alpha \\ -\sin\alpha & \cos\alpha \end{bmatrix} \begin{bmatrix} x_{\mathcal{S}} \\ z_{\mathcal{S}} \end{bmatrix} \tag{2}$$

For contour following, we are only interested in the normal distance x_N. Given that we have three barometers on a whisker, our hypothesis function is given by:

$$h_\theta(b) = \theta_0 + \theta_1 b_1 + \theta_2 b_2 + \theta_3 b_3 \tag{3}$$

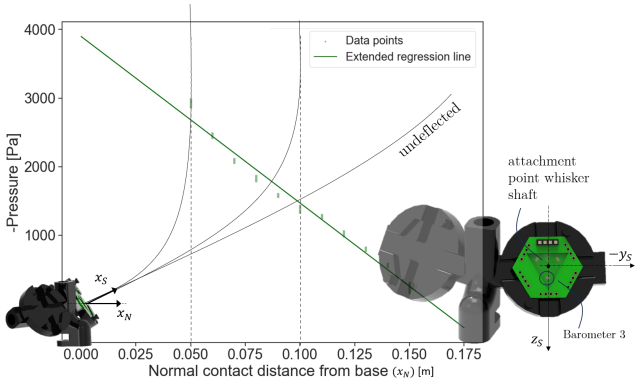

Figure 6 Results of static calibration set-up for barometer 3 of one whisker. Linear regression with approximately 10,000 data points (R^2 value of 0.98 and RMSE of 105 Pa). During calibration, the whisker is placed in the same connector as on the aerial platform to ensure consistency.

Where b_i is the pressure value associated to each barometer. However, from our assumption that bending only occurs in the xz-plane of the $\{\mathcal{S}\}$ frame, and that this bending direction aligns with barometer 3, we can simplify this hypothesis function to:

$$h_\theta(b_{3_j}) = \theta_0 + \theta_3 b_{3_j} \tag{4}$$

For each training sample j, or in matrix form:

$$\vec{\mathbf{h}_\theta}(\mathbf{B}) = \mathbf{B}\vec{\theta} \tag{5}$$

where $\mathbf{B}$ is the matrix of input features (pressure readings from barometer 3) with an added column of ones for the intercept. We arrive at the normal equation for our simplified system:

$$\vec{\theta} = (\mathbf{B}^T\mathbf{B})^{-1}\mathbf{B}^T\vec{\mathbf{x}}_N \tag{6}$$

Solving Equation 6 yields optimal parameters $\{\theta_0, \theta_3\}$. θ_0 is tuned in-flight such that the normal distance is estimated w.r.t the body frame of the aerial platform. We call this distance $x_\mathcal{B}$, where $\{\mathcal{B}\}$ denotes the body reference frame of the quadcopter, as shown in Figure 4.

The pressure readings are zeroed before data is collected for contact at different normal distances from the sensor base (x_N). Data is collected by placing a box at known distances from the whisker base, simulating contact with a wall. Measurements are taken in 0.01 m increments, ranging from 0.05 m to 0.15 m from the base. Linear regression of the whisker data resulted in R^2 values ranging from 0.89 to 0.98, and Root Mean Squared Error (RMSE) values between 26 Pa and 105 Pa, depending on the whisker. Discrepancies are primarily due to manufacturing variations, particularly in how the resin flows during manufacturing. Since there is limited control over the resin's distribution around the PCB, the resin coverage on and around the barometers may vary between whiskers.

While this 1D model is suitable for the environment considered in this research, out-of-plane deflections occurring when contact is made with curved surfaces could lead to inaccuracies. This issue is further discussed in Section 6.

4.3 Contour following controller design

Before entering the contour following state, the orientation of the wall is estimated. This is done by using the difference in estimated normal distance between the two whiskers from the contact event that triggered the surface evaluation state (see Figure 7). This estimated orientation is sent as a yaw command to the autopilot before making contact with the wall again, such that the whiskers are perpendicular to the wall during contour following.

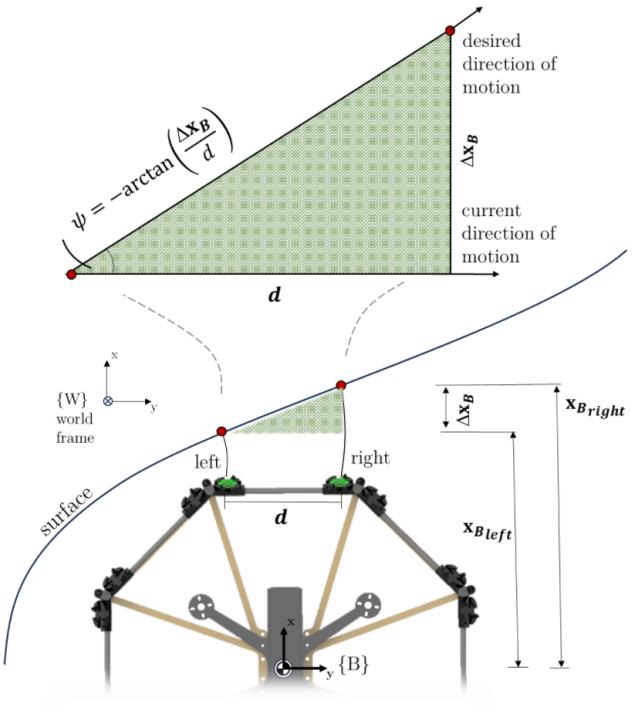

Figure 7 Surface Evaluation State - The drone estimates the orientation of the surface from a single contact event by calculating the difference in normal distance estimation between the two whiskers.

The contour following controller uses a single whisker as input to provide reference positions to the PX4 position controller. Figure 8 illustrates how this reference position is determined. During testing, we found that the PX4 position controller was not responsive enough to small and sudden changes in position inputs (A more detailed comment on the limitations of the position controller is given in Appendix B). As such, we were not able to directly use the error as a position command. Instead, we chose to supply a fixed corrective

action x_{input} of ± 0.01 meters when the estimated normal distance to the wall exceeded the deadband of ± 0.03 meters and apply a smoothing filter. This is done by means of an exponential moving average filter ($\alpha = \frac{2}{N+1}$, with $N = 20$) to smooth the inputs and determine the reference position provided to the position controller. Thus, the filtered reference position is given by:

$$\vec{\mathbf{p}}_{i+1_{EMA}} = \vec{\mathbf{p}}_{i+1}\alpha + (1-\alpha)\vec{\mathbf{p}}_{i_{EMA}} \tag{7}$$

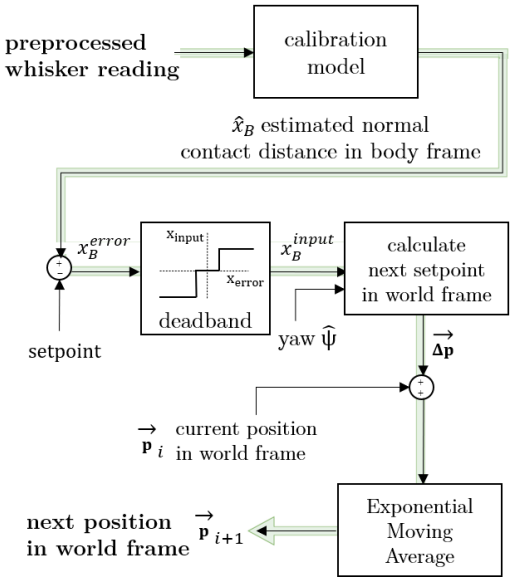

Figure 8 Contour Following Controller Logic. The drone moves parallel to the surface. This direction is determined by the estimated orientation in the surface evaluation state and corresponds to the drone's yaw angle ($\hat{\Psi}$). The preprocessed whisker data is linearly transformed into an estimated normal distance from the wall by the calibration model. If this distance deviates by more than ± 0.03 meters from the setpoint (deadband), a corrective position input ($x_{\mathcal{B}}^{input}$) is supplied to adjust the drone's normal distance from the wall.

5 Experiments

In this section we perform a system demonstration of the contour following capabilities of the proposed whisker-based aerial sensing platform.

5.1 Set-up

The experiments take place in an indoor drone arena equipped with OptiTrack Motion Capture cameras. The optitrack position estimate is communicated via ROS2 to the PX4 autopilot to be used by the on board EKF2 state estimator. The set up of the experiment is as shown in Figure 9. Mattresses are placed near the wall for softer landing. The following coordinates are given in the World-frame

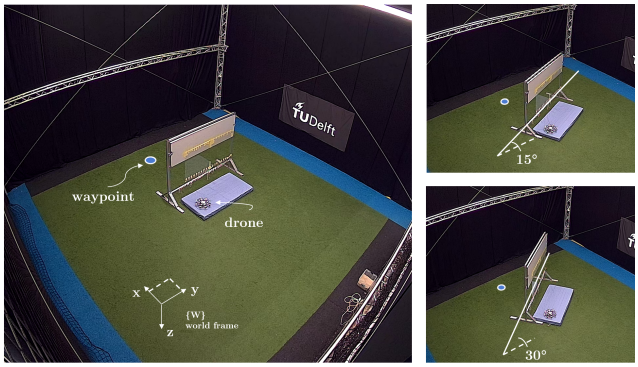

Figure 9 Drone arena experimental set-up for system demonstration. Wall oriented at three different angles: 0°, 15°, 30°.

{W}. The drone takes off from $\vec{\mathbf{p}}_0 = \{0.00, 0.00, -0.27\}^T$ meters to $\vec{\mathbf{p}}_{to} = \{0.00, 0.00, -1.80\}^T$ meters. Once the altitude is reached, the finite state machine is initialized. After calibration, the drone navigates to the supplied waypoint $\vec{\mathbf{p}}_{wp} = \{2.00, 0.00, -1.80\}^T$. Between the take-off position and the waypoint, a wall of length 2.5 meters is placed. Fifteen flights were performed at three different wall orientations with respect to the forward direction of the drone (45 flights in total). Given the right-handed coordinate system used, these orientations were $\Psi = \{0°, -15°, -30°\}$. In the contour following state the controller follows the wall for 2.0 meters, after which the drone enters the land state to conserve battery and returns to the position $\vec{\mathbf{p}}_{land} = \{0.00, 0.00, -0.30\}^T$ to land. Before each flight, a new setpoint is given to the controller for the contour following state. This setpoint is randomly sampled from $X \sim U(0.24, 0.34)$.

5.2 Results

	0 °	**15 °**	**30 °**	**All Flights**
RMSE				
Normal distance estimation [m]	0.021	0.025	0.030	**0.026**
Wall orientation estimation [°]	8.8	5.0	5.7	**6.8**
Standard Deviation				
Normal distance estimation [m]	0.019	0.024	0.030	**0.025**
Setpoint tracking [m]	0.037	0.039	0.045	**0.041**

Table 2 Summary of performance metrics for distance estimation, wall orientation estimation, and setpoint tracking. The accuracy of normal distance estimation consistently exceeds the setpoint tracking accuracy of the PX4 position controller, indicating that this simple linear calibration model provides sufficient accuracy for aerial navigation.

Figure 10A illustrates the FSM states and transitions during a flight test with a wall orientation of 15°. Only one whisker is used during the contour following phase. The con-

tour following trajectory setpoints and the resulting odometry for this flight are shown in Figure 10B. Due to the PX4 position controller's inability to maintain centimeter-level accuracy, fluctuations in whisker readings are observed. Nevertheless, the calibration model estimates the distance to the wall with sufficient accuracy, given the controller's tracking performance. These results validate the success of the FSM framework employed in this study and suggest potential for further research within each state.

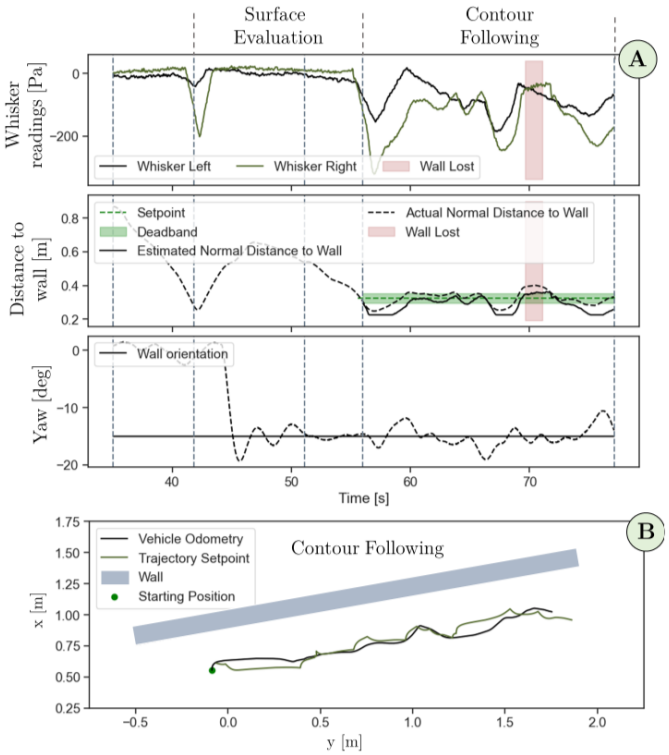

Figure 10 **—A:** Finite State Machine (FSM) states and transitions based on whisker data with a wall orientation of 15°. In the first half of the Surface Evaluation state, the drone infers the wall's orientation. In the second half (denoted by the dashed line), a second contact event is attempted. The difference in pressure between the left and right whiskers during the transition from waypoint navigation to surface evaluation is used to estimate the wall's orientation, leading to an adjustment in yaw. These results highlight the importance of our calibration model, which maps whisker readings to 1D contact locations, as pressure readings differ between the whiskers even when perpendicular to the surface. Our FSM framework demonstrates the ability to successfully detect contact, infer orientation, and estimate the normal distance to the wall during contour following. **—B:** Contour Following State trajectory setpoints and odometry for the flight shown in A. The right whisker is used for wall following. The PX4 position controller's inability to maintain centimeter-level accuracy results in the fluctuations observed in whisker readings in subfigure A.

Figure 11A shows specifically the contour-following results from one flight-test with wall orientation 0°. Figure 11B presents the error between the actual and estimated normal distances for the example in Figure 11A. Generally, the error is maintained within a 0.02-meter range. However, the large error at around 4 seconds suggests that near the whisker base the behaviour may not be linear. However, these results demonstrate the effectiveness of a simple linear mapping from pressure to 1D normal distance.

In Figure 11C and 11D, we plot the normal distributions of calibration model error across all flights. In the former we aggregate the results for all the flights and compute the mean and the standard deviation of the results. In the latter we do the same, but per wall orientation. Notably, the error is generally lower than the setpoint tracking error of the PX4 position controller, indicating that the accuracy of this simple calibration model is sufficient for aerial navigation. This can be seen in Table 2, which summarizes the results of normal distance estimation, wall orientation estimation, and setpoint tracking performance across all flights. The RMSE for the 0° orientation estimation is higher due to one flight where the drift correction for one of the whiskers was underestimated, resulting in an estimated orientation of around -28°. Excluding this flight, the RMSE would decrease to approximately 4.90°. Considering this, we can conclude that the performance of distance estimation degrades with increasing wall orientation. This is due to the contact event between the whisker and the surface deviating from the static calibration model, which assumed that the whisker would deflect only around its local y-axis. However, as wall orientation increases, lateral slip against the surface occurs. This out-of-plane contact event leads to less accurate wall orientation and distance estimations, as the whisker's orientation with respect to the surface becomes less perpendicular. Since this distance estimation is an input for the contour following controller, the standard deviation of setpoint tracking increases. However, with a deadband of ±3 cm, the standard deviations for setpoint tracking are within expected limits. These results demonstrate that this non-intrusive perception strategy is suitable for real-time navigation tasks for aerial platforms.

6 Future Work

Future research could extend from this work in several directions:

6.1 Sensor model that includes out-of-plane deflections

Extending the static calibration setup to account for lateral slip by incorporating an additional barometer into the regression process could significantly improve the accuracy of the sensor readings, particularly on surfaces with steeper angles. By integrating this additional barometer and including angled surfaces into the static calibration setup, the system could more effectively detect and correct for lateral movements, thereby reducing the error observed during contact with inclined surfaces. Furthermore, augmenting the plat-

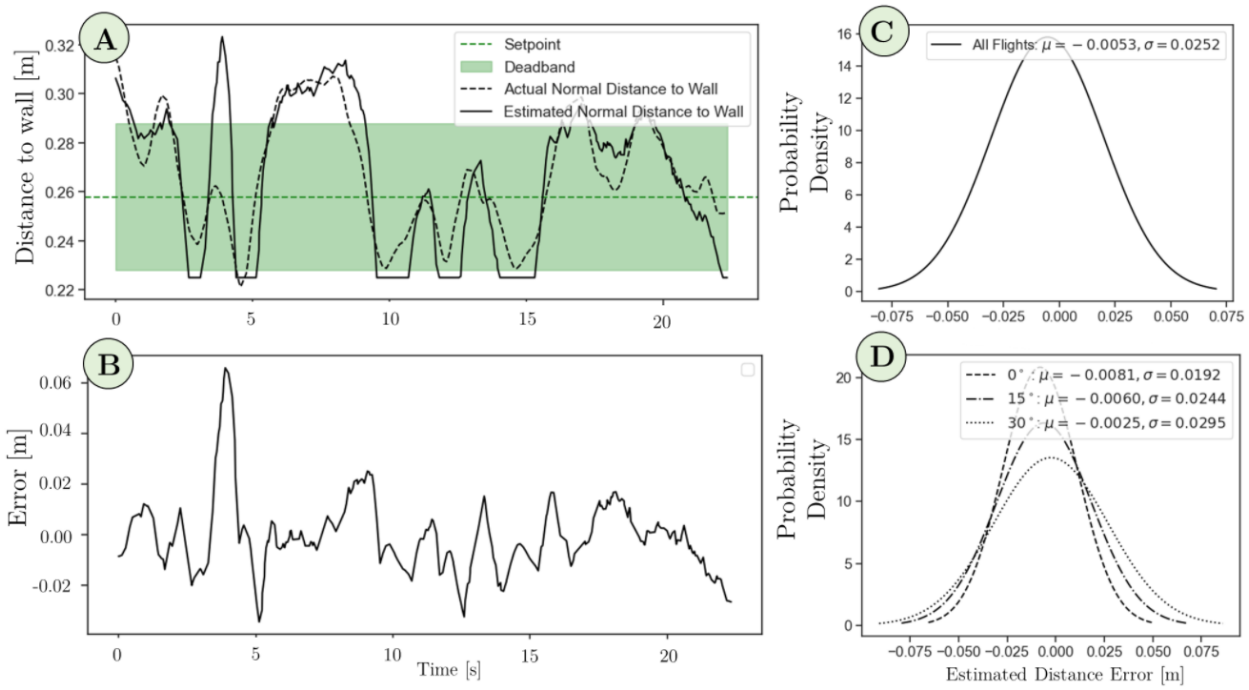

Figure 11 **—A:** Contour following results from a single flight with a wall orientation of 0°. The estimated normal distance ($x_{\mathcal{B}}$) is relative to the body frame. The plateau at 0.225 meters is due to a constraint setting any distance below 0.225 meters to this value, reflecting the distance from the drone's center of gravity to the whisker base. **—B:** Distance error from plot A, with a significant error around 4 seconds, indicating potential non-linearity near the whisker base. **—C:** Normal distribution of estimated distance errors during contour following across all flights. **—D:** Normal distribution of distance errors by wall orientation, showing increased standard deviation with orientation due to more lateral slip.

form with additional sensors—such as in the positions shown in Figure 4 could provide even more comprehensive coverage. These additional whiskers would be especially beneficial for decreasing the occurrence of lateral slip during the surface orientation estimation at higher angles. This enhanced sensor array could lead to improved overall accuracy of the platform when navigating and interacting with complex environments. Additionally, exploring non-linear models could improve the accuracy of distance estimation, particularly when the platform is in close proximity to the surface.

6.2 Towards pose estimation and SLAM

We can conceptualize the level of perception in robotic systems as existing on a spectrum that ranges from basic binary obstacle detection to sophisticated Simultaneous Localization and Mapping (SLAM). As we progress along this spectrum towards more advanced capabilities like pose estimation and SLAM, we could leverage the Extended Kalman Filter (EKF) solution presented in [12]. In this work, contact localization is achieved by defining a process model that allows for precise tracking of the contact point over time. The process model is given by the following equation:

$$x_{k+1} = \boldsymbol{A}x_k + \boldsymbol{B}\begin{bmatrix} \boldsymbol{v}^s_{ws} \\ \omega^s_{ws} \end{bmatrix} + \boldsymbol{w}_k \tag{8}$$

Where the notation v^a_{ab} is the linear velocity of reference frame A relative to B (subscript) as viewed in the reference frame A (superscript). {W} and {S} denote the world and the sensor frame respectively, ω_k is process noise and $\mathbf{x}_k$ is the contact location $\mathbf{p}_c$.

The velocity of the contact point in the body frame $\{\mathcal{B}\}$ is derived as [1]:

$$\boldsymbol{v}^b_{bp_c} = -\begin{bmatrix} \boldsymbol{I} & [\boldsymbol{p}_c] \end{bmatrix}\begin{bmatrix} \boldsymbol{v}^b_{wb} \\ \boldsymbol{\omega}^b_{wb} \end{bmatrix} \tag{9}$$

The linear and angular velocities $\boldsymbol{v}^b_{wb}$, $\boldsymbol{\omega}^b_{wb}$ are accessible through the PX4 state estimator. We can also say that:

$$\boldsymbol{x}_{k+1} = \boldsymbol{x}_k + \delta_t \boldsymbol{v}^b_{wp_c} \tag{10}$$

This leads to $\boldsymbol{A} = I$ and $\boldsymbol{B} = -\delta_t \begin{bmatrix} \boldsymbol{I} & [\boldsymbol{p}_c] \end{bmatrix}$. By combining this process model of the contact point, with the sensor model (derived in subsection 4.2), we can track contact locations from a sequence of measurements through Bayesian filtering.

$$\begin{aligned} b(\boldsymbol{x}_t) &= p(\boldsymbol{x}_t \mid \boldsymbol{z}_{1:t}, \boldsymbol{u}_{1:t}) \\ &= \eta p(\boldsymbol{z}_t \mid \boldsymbol{x}_t, \boldsymbol{u}_t) \int p(\boldsymbol{x}_t \mid \boldsymbol{x}_{t-1}, \boldsymbol{u}_t)\, b(\boldsymbol{x}_{t-1})\, d\boldsymbol{x}_{t-1} \end{aligned} \tag{11}$$

[1] Refer to [12] for the full derivation.

This recursive algorithm estimates the state distribution based on a history of control inputs and sensor data. In the equation, η is a normalization factor, $b\left(x_{t-1}\right)$ represents the prior distribution, and the terms $p\left(\boldsymbol{z}_t \mid \boldsymbol{x}_t, \boldsymbol{u}_t\right)$ and $p\left(\boldsymbol{x}_t \mid \boldsymbol{x}_{t-1}, \boldsymbol{u}_t\right)$ are derived from the sensor model and process model, respectively. By incorporating this EKF-based approach, we can more accurately estimate the contact point and enhance its ability to map the environment in real-time. This method represents a significant step forward in advancing to a more nuanced and comprehensive understanding of the environment, enabling the robot to operate with greater autonomy and precision in complex settings.

6.3 More robust preprocessing

While advanced static calibration and improved contact localization methods would enhance system accuracy and help mitigate lateral slip, the success of these models fundamentally relies on consistent data preprocessing across all flights. Uniform preprocessing is crucial for the reliability and effectiveness of these approaches. Developing a more robust filter for drift correction holds significant potential, as it would improve contact localization accuracy and overall system precision under varying flight conditions. Currently, drift correction is applied throughout the flight, and refining this process would likely increase sensor model accuracy. Additionally, it is important to consider the impact of linear and angular accelerations on drift. A high-pass filter is currently used to attenuate these effects at low speeds, but a deeper understanding of how platform dynamics influence sensor readings could facilitate the transition toward using the whiskers for pose estimation.

6.4 Controller

Transitioning from a position controller to a lower-level control mechanism, such as a rate controller, could significantly reduce the standard deviation observed in wall-following tasks. This shift would help minimize the risk of intrusive contacts with the environment, thereby enhancing the safety and effectiveness of the system in practical applications. By providing more responsive and precise control, a rate controller could better manage the subtleties of maintaining consistent distances from surfaces, which is particularly important in complex or sensitive environments.

7 Conclusion

In this study, we showcased the potential of non-intrusive biomimetic vibrissal sensing for aerial robotics. We introduced a novel platform that facilitates easy integration of sensors and a real-time preprocessing solution to mitigate signal distortion caused by the platform. We demonstrated that a simple static calibration setup, combined with strategic whisker placement, effectively localizes contact for contour-following tasks using only whisker data. Our novel drone platform, equipped with two modular sensors, maintains a desired distance from a flat contour within 8 centimeters and estimates its distance within 5 centimeters, as well as the surface orientation within 13.5°—all with 95% confidence.

This work marks the first successful integration of biomimetic vibrissal sensors into a modular aerial platform, setting a new standard in the field of tactile navigation for aerial robotics. By achieving real-time, online processing of tactile data for contact localization and surface orientation estimation, we have laid a solid foundation for future research in this domain. The modular and adaptable nature of the platform paves the way for further advancements, enabling more sophisticated applications such as exploration in cluttered environments or tactile mapping. This research not only demonstrates the feasibility of real-time tactile sensing in aerial platforms but also opens up new possibilities for enhancing robotic perception and interaction in complex, dynamic settings.

References

[1] Shan Luo, Joao Bimbo, Ravinder Dahiya, and Hongbin Liu. Robotic tactile perception of object properties: A review. *Mechatronics*, 48: 54–67, December 2017. ISSN 0957-4158. doi: 10.1016/j.mechatronics.2017.11.002. URL https://www.sciencedirect.com/science/article/pii/S0957415817301575.

[2] S.B. Vincent. The function of the vibrissae in the behavior of the white rat. *Animal Behavior Monographs*, 1, 5:84–84, 1912.

[3] W. I. Welker. Analysis of Sniffing of the Albino Rat. *Behaviour*, 22(3/4):223–244, 1964. ISSN 0005-7959. URL https://www.jstor.org/stable/4533073. Publisher: Brill.

[4] Marcin Szwed, Knarik Bagdasarian, Barak Blumenfeld, Omri Barak, Dori Derdikman, and Ehud Ahissar. Responses of trigeminal ganglion neurons to the radial distance of contact during active vibrissal touch. *Journal of Neurophysiology*, 95(2):791–802, February 2006. ISSN 0022-3077. doi: 10.1152/jn.00571.2005.

[5] Cagdas Tuna, Douglas L. Jones, and Farzad Kamalabadi. Tactile tomographic fluid-flow imaging with a robotic whisker array. In *2014 IEEE International Conference on Acoustics, Speech and Signal Processing (ICASSP)*, pages 6815–6819, May 2014. doi: 10.1109/ICASSP.2014.6854920. ISSN: 2379-190X.

[6] William Deer and Pauline E. I. Pounds. Lightweight Whiskers for Contact, Pre-Contact, and Fluid Velocity Sensing. *IEEE Robotics and Automation Letters*, 4(2):1978–1984, April 2019. ISSN 2377-3766. doi: 10.1109/LRA.2019.2899215. Conference Name: IEEE Robotics and Automation Letters.

[7] Suhan Kim, Regan Kubicek, Aleix Paris, Andrea Tagliabue, Jonathan P. How, and Sarah Bergbreiter. A Whisker-inspired Fin Sensor for Multi-directional Airflow Sensing. In *2020 IEEE/RSJ International Conference on Intelligent Robots and Systems (IROS)*, pages 1330–1337, October 2020. doi: 10.1109/IROS45743.2020.9341723. ISSN: 2153-0866.

[8] Charles Fox, Ben Mitchinson, Martin Pearson, Anthony Pipe, and Tony Prescott. Contact type dependency of texture classification in a whiskered mobile robot. *Autonomous Robots*, 26:223–239, May 2009. doi: 10.1007/s10514-009-9109-z.

[9] Moritz Scharff, Alencastre Jorge, and Carsten Behn. Detection of Surface Texture with an Artificial Tactile Sensor. In *Mechanisms and Machine Science*, pages 43–50. January 2019. ISBN 978-3-030-16422-5. doi: 10.1007/978-3-030-16423-2_4. Journal Abbreviation: Mechanisms and Machine Science.

[10] Joerg Hipp, Ehsan Arabzadeh, Erik Zorzin, Jorg Conradt, Christoph Kayser, Mathew E. Diamond, and Peter König. Texture Signals in Whisker Vibrations. *Journal of Neurophysiology*, 95(3):1792–1799, March 2006. ISSN 0022-3077. doi: 10.1152/jn.01104.2005. URL https://journals.physiology.org/doi/full/10.1152/jn.01104.2005. Publisher: American Physiological Society.

[11] Mahima Yoga. Whisker-inspired Tactile Sensing for Robots.

[12] Michael Lin, Emilio Reyes, Jeannette Bohg, and Mark Cutkosky. *Whisker-Inspired Tactile Sensing for Contact Localization on Robot Manipulators*. October 2022. doi: 10.48550/arXiv.2210.12387.

[13] Chaoxiang Ye, Guido de Croon, and Salua Hamaza. A Biomorphic Whisker Sensor for Aerial Tactile Applications. *2024 IEEE International Conference on Robotics and Automation (ICRA)*. URL https://tacyee.github.io/images/ICRA-2024_Chaoxiang%20Ye_Final_2.pdf.

[14] Chenxi Xiao, Shujia Xu, Wenzhuo Wu, and Juan Wachs. Active Multiobject Exploration and Recognition via Tactile Whiskers. *IEEE Transactions on Robotics*, 38(6):3479–3497, December 2022. ISSN 1941-0468. doi: 10.1109/TRO.2022.3182487. Conference Name: IEEE Transactions on Robotics.

[15] Charles Fox, Mat Evans, Martin Pearson, and Tony Prescott. Tactile SLAM with a biomimetic whiskered robot. In *2012 IEEE International Conference on Robotics and Automation*, pages 4925–4930, St Paul, MN, USA, May 2012. IEEE. ISBN 978-1-4673-1405-3 978-1-4673-1403-9 978-1-4673-1578-4 978-1-4673-1404-6. doi: 10.1109/ICRA.2012.6224813. URL http://ieeexplore.ieee.org/document/6224813/.

[16] Mohammed Salman and Martin J. Pearson. Advancing whisker based navigation through the implementation of Bio-Inspired whisking strategies. In *2016 IEEE International Conference on Robotics and Biomimetics (ROBIO)*, pages 767–773, December 2016. doi: 10.1109/ROBIO.2016.7866416.

[17] Mohammed Salman and Martin J. Pearson. Whisker-RatSLAM Applied to 6D Object Identification and Spatial Localisation. In Vasiliki Vouloutsi, José Halloy, Anna Mura, Michael Mangan, Nathan Lepora, Tony J. Prescott, and Paul F.M.J. Verschure, editors, *Biomimetic and Biohybrid Systems*, Lecture Notes in Computer Science, pages 403–414, Cham, 2018. Springer International Publishing. ISBN 978-3-319-95972-6. doi: 10.1007/978-3-319-95972-6_44.

[18] Tareq Assaf, Emma D. Wilson, Sean Anderson, Paul Dean, John Porrill, and Martin J. Pearson. Visual-tactile sensory map calibration of a biomimetic whiskered robot. In *2016 IEEE International Conference on Robotics and Automation (ICRA)*, pages 967–972, May 2016. doi: 10.1109/ICRA.2016.7487228.

[19] Miriam Fend. Whisker-Based Texture Discrimination on a Mobile Robot. pages 302–311, September 2005. ISBN 978-3-540-28848-0. doi: 10.1007/11553090_31.

[20] Yulai Zhang, Shurui Yan, Zihou Wei, Xuechao Chen, Toshio Fukuda, and Qing Shi. A Small-Scale, Rat-Inspired Whisker Sensor for the Perception of a Biomimetic Robot: Design, Fabrication, Modeling, and Experimental Characterization. *IEEE Robotics & Automation Magazine*, 29(4):115–126, December 2022. ISSN 1558-223X. doi: 10.1109/MRA.2022.3182870. Conference Name: IEEE Robotics & Automation Magazine.

[21] A.E. Schultz, J.H. Solomon, M.A. Peshkin, and M.J. Hartmann. Multifunctional Whisker Arrays for Distance Detection, Terrain Mapping, and Object Feature Extraction. In *Proceedings of the 2005 IEEE International Conference on Robotics and Automation*, pages 2588–2593, April 2005. doi: 10.1109/ROBOT.2005.1570503. ISSN: 1050-4729.

[22] Joseph Solomon and Mitra Hartmann. Extracting Object Contours with the Sweep of a Robotic Whisker Using Torque Information. *I. J. Robotic Res.*, 29:1233–1245, August 2010. doi: 10.1177/0278364908104468.

Part III

Literature Review

*This part has been assessed for the course AE4020 Literature Study.

[This page is intentionally left blank]

Whisker-inspired Tactile Sensing for Robots

M. Yoga, *m.h.yoganarasimhan@student.tudelft.nl*
Faculty of Aerospace Engineering, Delft University of Technology

ABSTRACT

Whisker/Vibrissae-inspired sensors are an emerging class of tactile sensors that mimic the vibrissal systems observed in nature. These sensors offer several advantages over traditional tactile sensors, including ease of manufacturing and non-invasiveness during operation. Biomimetic vibrissal sensors have a wide range of proven applications such as shape inference, navigation, texture discrimination, and fluid profile analysis. This review provides an overview of past and current research in the field of vibrissal sensing for robotics, including their design principles, morphologies, robotic applications and challenges. We argue that this novel tactile sensing scheme can bring the unique opportunity to continuously improve upon the sensory capacity of machine perception by closely aligning robotic modalities with ongoing research on the rat's sensorimotor system.

1 INTRODUCTION

Tactile sensing is an essential component of a robot's ability to interact with its environment. It enables robots to detect and identify objects, navigate through complex environments, and manipulate objects with precision [1]. Tactile sensors have been used in robotics for decades, but the development of new sensor technologies and their integration with advanced control algorithms have led to significant improvements in robotic tactile perception.

One domain of research that has garnered interest in recent years is the use of biomimetic vibrissal sensors for tactile perception in robotics. Whiskers are specialized sensory organs found in many mammals, including rodents, seals, and cats. These structures are used for a variety of purposes such as navigation, prey detection, and social communication. Whisker-inspired sensors mimic the structure and function of natural whiskers and have several advantages over traditional tactile sensors. They are lightweight, low-power, and can operate in a wide range of environmental conditions. The reviewed literature demonstrates the potential to detect subtle changes in the environment, such as air currents, vibrations, and texture gradients. Arguably, one of the biggest advantages over traditional tactile sensors is that vibrissal sensors are non-intrusive, meaning that interaction with the environment does not require changing the state of said environment. Furthermore, unique environments such as smoke filled settings or covert operations in the dark may herald vibrissal sensing applications. These features make vibrissal sensing for tactile perception an intriguing sensory modality.

In robotics, whisker-inspired sensors have been used in a variety of applications, including object recognition, navigation, surface exploration, and velocity profiling. The use of such sensors for tactile perception in robotics is still a relatively new area of research [2], and many challenges remain. This review paper explores the past and current adoption of vibrissal sensors in robotics, and the challenges that are faced.

The structure of the review is as follows. First, whisker-based tactile perception in nature is briefly introduced in **Section 2**. In **Section 3** an overview of whisker design is presented. Careful consideration is given to choice of material, geometry, transducer, actuation and array morphology of the sensing system for a given robotic application. Throughout the paper, four robotic applications are explored: *shape inference, navigation, texture discrimination* and *fluid flow analysis*. The various implementations of the sensors are thoroughly discussed for all four robotic applications in **Section 4**. Throughout the discussion, challenges within the specific application domain are considered. Finally, the global challenges and opportunities that exist for vibrissal sensing for robotic applications are discussed in **Section 5**.

2 WHISKER-BASED TACTILE PERCEPTION IN BIOLOGICAL SYSTEMS

The vibrissal system of rats has long been employed as a classic model in neuroscience for investigating the mechanisms of sensorimotor integration and active sensing [4, 5]. Whiskers, or vibrissae, are an essential part of many animals' sensory systems. These specialized hairs provide tactile information about the environment in which the animal explores.

The arrangement of whiskers can vary between different animals. Rodents, such as mice and rats, have long, conical, stiff whiskers arranged in rows on their faces [2, 3, 6]. Of approximately 30 macrovibrissae , the longest whiskers are typically found on the top row, with shorter whiskers on the lower rows [7]. Cats have whiskers located on their cheeks, eyebrows, and chin, and use them for social communication with other cats. Different positions of the whiskers convey different meanings. In contrast to rodents, cat whiskers are shorter and have a higher taper ratio, allowing more precise sensing of small movements [8]. Seals and other marine mammals have whiskers that are used to detect prey in the water [9]. These whiskers have elliptical cross-sections, and

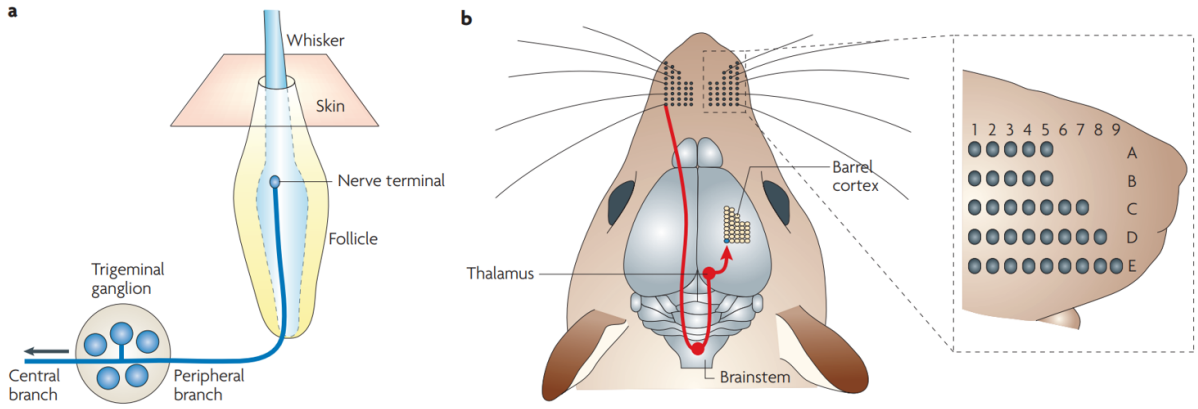

Figure 1 Sensory pathway layout of the whisker [3]. **—a:** schematic illustration of a mechanoreceptor terminal. **—b:** illlustration of the 2D grid formed by the vibrissae. Arranged in five rows (A-E), each including five to nine whiskers (1-9).

are arranged in an irregular pattern [2].

A schematic of a rodent's sensory pathway layout is given in Figure 1. The bending of the shaft is converted to a neural signal by mechanoreceptors situated in the follicle [10]. These signals are brought together in the primary afferent neurons of the brainstem trigeminal nerve. A schematic of this is given in Figure 1a. Information on direction, velocity, duration of whisker displacements and torques are encoded in these neurons [10], and enable rodents to localize objects, infer size, shape, orientation and texture with high precision [11–17]. Before reaching areas of the brain involved in memory, spatial mapping, and decision making, sensory signals generated by whisker stimulation travel from primary afferent neurons to different processing stations in the brainstem, midbrain, cerebellum, and forebrain [6]. *Barrels* are cellular aggregates of neurons in the primary somatosensory region of the rat cortex. These aggregates have a somatotopic one-to-one mapping with the whiskers [6]. In other words, each whisker has a corresponding "barrel" of neurons in the brain that responds to its stimulation. This is shown in Figure 1b. The existence of these barrels (often referred to as the *barrel cortex* [18]) makes it easier to identify and study the processing of vibrissal sensory signals in the brain.

"Whisking" is a rhythmic, controlled motion of the vibrissae that rodents perform during tactile exploration [19]. Whisking occurs at frequencies between 5-25Hz [7], and is speculated to differ between tasks [6]. For example, exploratory whisking exhibits different patterns when compared to 'free-whisking' [20]. Specifically, observations [20] have shown differences in 'spread' between whiskers during object contacts. These whisking behaviours are believed to stem from a 'Central Pattern Generator' (CPG) [21], of which the specific location within the rodent's body is yet to be pinpointed. By using movement to acquire and refine incoming sensory data, sensing is considered an 'active' process [7]. This process is thus, aside from the signal processing that occurs, heavily dependent on the material, mechanical, and morphological characteristics of the vibrissal system. Such characteristics include (but may not be limited to) stiffness [22, 23], resonant frequencies [24], damping [24], 3D morphology [7] and geometry [23, 25]. As such, mimicking this behaviour for applications in robotics is a challenging, but compelling, objective. The sensorimotor system of rodents remains one of the most actively researched fields. This brings the unique opportunity to continuously adapt and improve artificial sensors congruently.

3 Designing Vibrissal Sensors

Recently, a review on designs and manufacturing methods of whisker-inspired sensors was published [2]. This review provides in depth explanations and analyses of material and sensor design choices that have been made in literature. Thus, this section will focus on trends and provide a more global overview of designing vibrissal sensors for robotics.

3.1 Whisker Design

Sensor design varies in literature based on the goals of the research. The length, material and geometry of the whisker are most affected by what conclusions are to be drawn from the data the whisker sensor aims to collect. For example, a thin, tapered whisker may be more conducive to texture discrimination [23]. However, such a sensitive design may not be required for applications in which more global conclusions are to be drawn from the environment, for example SLAM. Furthermore, a portion of available literature focuses on biomimetic vibrissal sensors as a 'proof of concept' and places an emphasis on signal processing. As such, the design is often arbitrary and conclusions can not always be drawn between application and sensor design choices.

We observe the following generalized design across most published literature: the *whisker shaft* (a (tapered)

straight/curved beam), attached to a *follicle* (transducer). When an external load is applied to the whisker shaft, the experienced forces and moments result in a deformation at the follicle. This signal is thus measured by the transducer. The sensitivity of the sensor depends on material and geometric properties of the shaft, as well as the chosen transducer. The desired sensitivity is dependent on the robotic application. Exceptions to this standard design do exist. For example, vision based [26–28] methods do not directly measure signals due to deformation, but track specific features in an image. *Seth et al.* [29] implemented a sensor in which the shaft was made of two polyamide strips adhered back-to-back such that bending could be measured along the entire whisker shaft. *Schlegl et al.* [30] proposed 'virtual whiskers' formed by an electric field, where detection of objects did not require any contact. Figure 2 visualizes the observed trends in application - transducer - shaft material combinations found in literature. Newer applications, such as fluid flow and navigation, make use of polymer shafts more frequently. Shape inference, one of the most researched applications for vibrissal sensing in robotics, makes use of steel shafts often. The strain gauge is the most commonly used transducer, and is also used across all four applications. Second to this is the hall effect sensor; used primarily in more recently published literature. Both of these sensors have a bandwidth that is conducive to all applications. Finally, it may be noteworthy to mention that microphones and barometers have only been used with real vibrissae and polymers respectively. Table 1 maps the combinations of commonly used transducers and applications as found in literature. Binary whiskers and potentiometers [31] are the most simple transducers used. Binary whiskers are only able to distinguish between contact and no-contact scenarios based on an electrode at the base of the whisker shaft. As such, they are suitable for object detection applications. Potentiometers measure the torque of the whiskers due to contact, and are mostly paired with steel whiskers [32]. Due to their size and cost, strain gages are one of the most commonly used sensors across all applications. By placing them at the follicle, the resistance of the whisker (bending moment) to an external force is measured. Often, the strain gages are placed in a wheatstone bridge. This arrangement of multiple strain gages also allows for directionality in the measurements, which is not achievable with electret microphones [6]. However, durability and excessive noise may pose issues. Hall effect sensors measure the variations in the magnetic field due to the deformation of the follicle. Magnets are attached to the whisker base which is mounted above the hall effect sensor. The deformation of the whisker base (due to the moment) will cause the magnet to displace with respect to the sensor. As such, the sensitivity of the sensor is adjustable. The transducer that can provide the most information is the six-axis force/torque load cell. Load cells are able to measure all three components of the forces and moments at the base. Though accurate, load cells tend to be expensive and bulky. As can be seen in Table 1, load cells are most commonly used for shape inference/contour extraction experiments. These experiments tend to be isolated – meaning less consideration is given to scalability of the whisker into an array, or ensuring suitability for platform integration. Recently, MEMS barometers have been used [33, 34] as transducers (shown in Figure 3-I1). These pressure sensors are lightweight, small, and can achieve high accuracy. However, they are prone to drift [34]. For texture discrimination and fluid flow, where the frequency response of the sensor is valuable, the bandwidth of the transducer is important [35]. With a larger bandwidth, the high frequency vibrations at the tip of whisker are captured. Microphones (high cutoff frequency in the tens of kHz [35]) are thus very appropriate for texture discrimination. Strain gages, load cells, MEMS barometers, and hall-effect sensors have a moderately large bandwidth (10-1000Hz [35]), and are also suitable for other applications as they are able to capture low frequencies. This makes these transducers appropriate choices for multi-modal applications. Microphones have a low cutoff frequency of around 10-Hz, making them unsuitable for low frequency applications such as navigation and shape inference.

	Texture Discrimination	Shape Inference	Navigation	Fluid Flow Profiles
Binary			[31]	
Strain Gage	[36][37][38]	[39][36][38] [40][41][42][43]	[38]	[42][44]
Hall Effect	[45][46]	[47][48][49]	[50][51] [52] [49]	[53]
Force/Torque Load Cell	[54]	[55][56][57][58][59]		
Potentiometer		[32]	[31]	
Microphone	[22][60] [61] [62] [63]		[64][61][65]	
Barometer		[34]	[34]	[33]
Vision-Based		[66]		[26][27]
Piezoelectric	[46]	[48]		[67]
Accelerometer	[35]			

Table 1 Mapping of transducer used in Literature by Experiment

Regarding material choice for the whisker: a trade-off exists between sensitivity and durability. Rigid materials may lead to damage of the environment and of the sensor, as the reactions experienced at the base will be higher. Highly flexible materials may delay the reaction at the follicle (base) of the whisker due to lower/no reactions for a given whisker deflection [22, 38]. In a study performed by *Fend et al.* [65], an evolutionary algorithm came to various whisker morphologies using rigid and flexible whiskers for obstacle avoidance and exploration purposes. With flexible whiskers, more variety of whisker morphologies were found than with a rigid whisker. In addition, rigid whiskers evolved to be shorter when compared to flexible whiskers.

Materials used in research range from real rat vibrissae [22, 60], to a variety of metals (steel [31], aluminium [35], copper [36], nitinol [47]) to polymers [28] and composites [33]. Early research [31, 32] made use of steel wires as

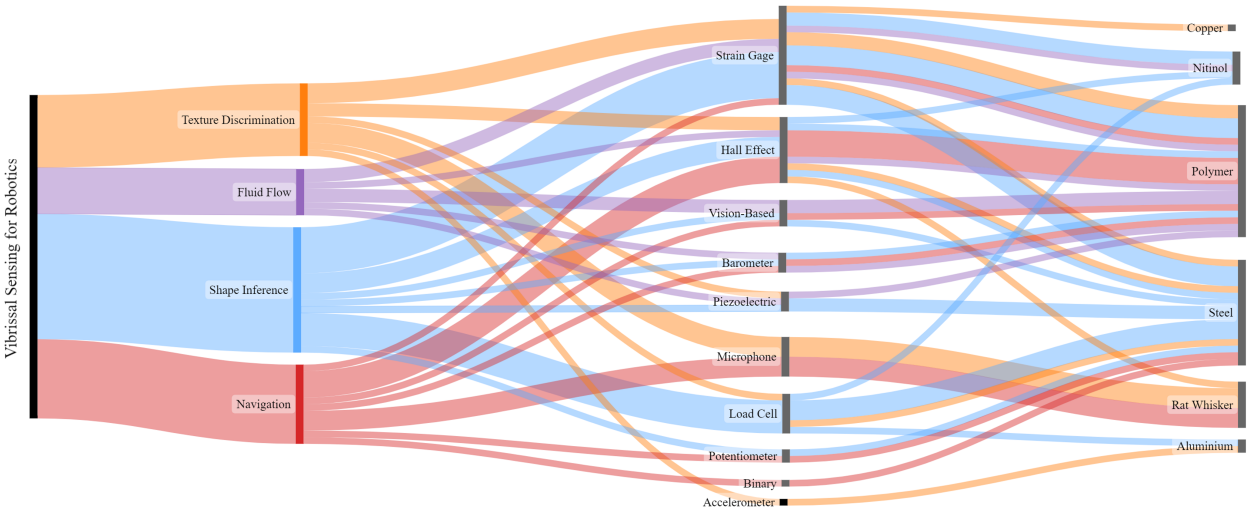

Figure 2 Mapping of whisker design combinations found in literature for different robotic applications.

whisker shafts. Steel, however, is under-damped compared to real vibrissae [24]. More recently [44, 47] nitinol has been used. Nitinol is more flexible compared to steel, and exhibits better damping behaviour. For sensors that aim to more closely replicate geometry and material properties of real vibrissae [68], polymers and composites are used. Multi modal sensors (suitable for more than one robotic application) [26, 33, 34, 49] require a range of whisker shaft characteristics that are conducive to different applications. For example, texture discrimination requires a stiff material for greater sensitivity when differentiating between surfaces [22]. For fluid flow applications, the shaft should be sufficiently sensitive such that even very small applied pressures are observable [69]. Thus, manufacturing whisker shafts in which the characteristics are highly tunable (as with composites) is beneficial for multi-modal sensors.

When considering whisker geometry, design choices can be made regarding the taper and curve of the whisker shaft. Using curved whiskers can have structural benefits, as they prevent supporting large axial loads and thus are able to avoid buckling [32]. *Lin et al.* [47] also observed that curved whiskers can achieve better 'passive whisking', and are able to track object contours with a higher accuracy when compared to their straight counterparts. However, production of a curved whisker is not straight-forward and should be considered. Especially in array-morphologies, consistent geometries may be hard to achieve for all whiskers in the array. *Yokoi et al.* [61] conducted a thorough analysis on tapered whiskers. They found that the conical shape was more robust against mechanical stress and fractures. This allows for longer whiskers, and thus also a longer sensing range. In addition, tapered designs are often lighter. This may be beneficial for platforms, such as MAV's, in which weight may be a limiting design factor. For texture discrimination applications, the eigen-frequency of the shaft and the ability to transduce the frequency characteristic of the sensed surface is important. The conical whisker acts as a highly discriminating bandpass filter, displaying greater sensitivity towards specific frequencies and transmitting distinct modes of vibration with increased efficiency [61]. It has been suggested [23] that tapered whiskers have the advantage of more pronounced 'stick-slip' signals for texture discrimination. However, more so than curved whiskers, manufacturing tapered whiskers has proven to be challenging as conventional drawing, extrusion, casting and molding processes are not suitable [43]. Thus far in literature, tapered whiskers have been manufactured through methods [68] and materials [37, 70] that don't allow for optimum geometries [68, 71]. *Collinson et al.* [43] proposed a novel manufacturing method termed 'surface conforming fiber drawing' (SCFD) that is able to achieve higher aspect ratios and finer tip diameters. The tapered SCFD whiskered demonstrated improved contact point localization (median distance error 0.57cm) when compared to a cylindrical whisker (median distance error 1.3cm).

3.2 *Array Morphology*

Array morphologies are beneficial for maximising data collection. In literature, arrays implemented for shape inference usually consist of multiple identical whiskers mounted next to each other, and don't give much attention to specific morphologies. This is in contrast to navigation applications, where whiskers are more often arranged in a morphology that

aids in decision making. *Fend et al.* expanded on previous research on array morphologies [22] in a series of papers that explore optimal morphologies for navigation [60, 65]. Six different array morphologies were investigated for their performance in obstacle avoidance and exploration tasks. Contrary to what is often found in nature, the morphology that performed best had the long whiskers mounted towards the center of the 'head', with the lengths decreasing towards the back. The spread of the whiskers was around 20 degrees. Although opposite to what is found in nature, it is also intuitive that this morphology works best for this application - as mounting the larger whiskers towards the back (as in nature) would imply less obstacle detection right in front of the robot. In addition, objects located on the sides of the robot would be detected and avoided, even though the risk of collision with these obstacles is low when the robot is moving forward. This in turn would also reduce exploration, as many more false positive exist. The Bristol Robotics Labratory has published iterations of several standardised whiskered robots, mounted with array morphologies: *Whiskerbot [70], SCRATCHbot [72] and Shrewbot [73]*, each design building upon the previous. The most recent robot, Shrewbot, makes use of the modular BIOTACT sensor [68] (see Figure 3-I3), mounted onto a conical shaped 'head'. As the sensors are modular, they can be mounted in any desirable morphology onto the Shrewbot's head (Figure 3-S1). Compared to the SCRATCHbot, the main innovation is the morphology of the macrovibrissal array. Shrewbot has six rows of three columns of whiskers that are arranged in a circular pattern around its head. This is different from SCRATCHbot, which has its whiskers arranged in a linear pattern. The design of Shrewbot's whiskers emphasizes the radial symmetry of the macrovibrissae found in rats [73]. Shrewbot is used as a platform for investigation biomimetic morphology and control in vibrissal active touch [51]. The BellaBot [74] is another biomimetic whiskered robot platform, also consisting of a 'head', containing 20 identical whisker-inspired sensors, mounted onto a 5 DoF manipulator. The BellaBot (shown in Figure 3-S2) has demonstrated the ability to accommodate imperfections in the sensory map that may be a result of poor manufacturing or damages to the array. This is a compelling concept, as generally robot performance is increased when using arrays, but tactile sensors are prone to damage due to their constant interaction with the environment. In addition, when working with highly tapered or curved whiskers, manufacturing differences may give rise to differences in signals. Thus, such a system could allow for robust and continued use of vibrissal arrays in robotics.

3.3 Whisker Actuation

To achieve active sensing in artificial vibrissae, the sensors may be actuated by a miniaturised electric motor. Alternative approaches include actuation through 'muscle-like' properties such as shape-memory alloys [75], or 'air muscles' [41]. This is commonly referred to as 'active whisking'.

Passive whiskers (non-actuated) may be based on the vibrissae found on, for example, the lower limbs of cats [47]. Though easier to manufacture, a number of hurdles arise when using passive whiskers. The most prominent being that the number of contacts with an object is limited, as contacts are limited to one interaction, rather than multiple probes [47]. The second hurdle is that the movement of the whiskers becomes entirely dependent on the control actions of the mobile platform on which the passive whisker is mounted. Most mobile platforms are not tuned to maximise exploration for short range sensors such as whisker-inspires sensors. A controller may be implemented to alter the actions of the platform based on the signals obtained, as has been done in navigation applications [31, 37]. However, these control actions are generally less precise compared to the actuation of the whisker itself.

During whisking, differences exist between the patterns that are tracked. Simple actuation may include whisking through an arc. *Kim and Möller* [48] chose to whisk through an arc of 50° and added an additional 21° when contact was made with an object to increase contact events. *Sullivan et al.* implemented a more elaborate approach [68]. Two active sensing strategies were introduced: rapid cessation of protraction (RCP) and contact-induced symmetry (CIA). While RCP is a feedback control strategy that stops the forward protraction of the whiskers as soon as contact is made [76], CIA is a feedforward strategy that regulates the contacts on subsequent whisks by moving them asymmetrically after contact has been made. Two coupled oscillators (to allow for both in-phase and out-of-phase whisking of the two sides) were generated that could be perturbed by the environment. These strategies follow the 'minimal impingement, maximal contact' (MIMC) whisking concept termed in [76], where the animal attempts to make as many contacts as possible without allowing excessive bending of the whisker. *Pearson et al.* [73] suggest that the MIMC approach may also be useful for maximizing information quality in robotics, as contact events are usually normalized. Thus, with an increased number of contacts, the range of the data will be less varied.

Towal and Hartmann [19] investigated bilateral free-whisking behaviour when a rat's head and whisker movements occur simultaneously. They found that coupling exists between the head and whisker movements, as the rat compensates its head movements in order to process the information acquired by the vibrissae. Such coupling was implemented on the *Shrewbot* [51], where the movement of the head and body is coordinated with the whisker motion. They found that their control strategy promoted complex behaviour patterns such as exploration.

To conclude this design section, Figure 3 collates some of the designs proposed in literature. Each row focuses on either individual sensor designs (I1-I3), mounted sensors (M1-M4), or standardized array morphologies (S1-S2). In the caption,

information can be found on the main design choices, and the application for which they were used.

4 Applications in Robotics

4.1 Shape Inference

Shape inference and surface reconstruction for tactile sensors has drawn inspiration from both local and global computer vision algorithms. Local methods rely on shape descriptors/feature learning, and often use 'tactile images' to learn object classification. *Pezzementi et al* [79] presents a process to learn 'bag-of-features' models for each object class by using k-means clustering of data. Descriptors are extracted through methods such as the Scale Invariant Feature Transform (SIFT) [80] and MR-8 [81]. *Luo et al.* [82] proposed a tactile-SIFT algorithm in which local observations are used to perform global shape recognition. Global methods, such as point cloud methods [83], Gaussian process implicit surfaces (GPIS) [84] and Bayesian inference algorithms [85] aim to reconstruct entire object surfaces based on sparse data through probabilistic methods [86]. Recently, GPIS has been implemented by *Suresh et al.* [87] for tactile shape recognition and localization through planar pushing.

Early research by *Russel* [32] and *Wilson and Chen* [41] into surface reconstruction using a whisker-inspired sensor considered only contact at the tip of the whisker. 2D surface profiles were reconstructed from the known location of the mobile platform and the known angular deflection at the whisker base. By applying translations and rotations to these measurements, the location of the contact point with respect to the robot platform is known. Preliminary shape inference could then be achieved by plotting the contact localization points on a grid for a single whisker with multiple probing events. This method was able to track surface contours adequately for both concave and convex shapes. However, ensuring only object contact at the tip is tedious, and increases sparsity of data. Shape inference through tactile perception thus presents a dual challenge. The central aspect of this challenge revolves around the precise localization of contact forces along the whisker shaft. This critical step precedes the actual process of shape inference. Consequently, a significant portion of research within this domain is dedicated to addressing and refining the contact force localization problem.

Rodents possess both slowly adapting and rapidly adapting mechanoreceptors located around the whisker shaft within the follicle. Physiological evidence indicates that these receptors play a role in encoding signals related to deflection amplitude and velocity at the ganglion cell level [88, 89]. As such, this phenomenon is often modelled by using *elastica theory* [90], which relates the curvature of a deformable beam to the moment at its base [91].

The slope of a whisker-sensor resulting from the application of torque (τ) during a contact event can be determined using the Bernoulli-Euler equation, given by Equation 1. Where E and I are the Young's modulus and area moment of inertia

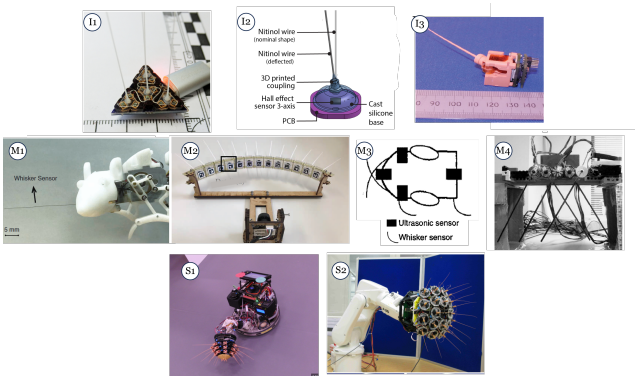

Figure 3 Collection of designs found in literature. Row I: individual whisker designs, Row M: whiskers mounted on a platform, Row S: standardized designs. **—I1:** non-actuated, tapered resin whisker shaft with MEMS barometer transducer designed for fluid flow, pre-contact sensing [33]. **—I2:** schematic of non-actuated nitinol whisker shaft with hall effect transducer designed for probabilistic shape inference [47]. **—I3:** actuated, tapered nanocure25 whisker shaft with hall effect transducer designed for simultaneous localisation and mapping (SLAM) [73]. **—M1:** non-actuated, nylon whisker shaft with strain gauge transducer mounted on a mobile rodent-inspired robot used for wall following, texture discrimination, and shape inference [38]. **—M2:** non-actuated, polyester whisker shaft with camera transducer mounted on an aerial platform used for obstacle avoidance [28]. **—M3:** schematic of non-actuated piano wire (front) and steel (side) whisker shafts with binary and potentiometer transducers respectively, mounted on a mobile robot used for obstacle avoidance and wall following [31]. **—M4:** non-actuated, nitinol whisker shaft covered with plastic straw with strain gauge transducer mounted on an test set-up for tomographic imaging of the air-flow [44]. **—S1:** standardised design "Shrewbot" using sensor described in I3 on mobile robot platform for tactile SLAM. Shrewbot consists of a Robotino [77] "body", an Elumotion [78] 3 DoF 'neck' and a custom built end-effector 'head' [51]. **—S2:** standardised design "BellaBot". Actuated, tapered nanocure25 whisker shaft with hall effect transducer. BellaBot consists of a custom built "head" that holds an array of 20 whiskers on a 5DoF industrial manipulator used for tactile sensory map calibration. [74]

of the whisker shaft respectively, x is the position along the whisker shaft, x_c is the distance of the contact point from the base of the whisker and $\tan\theta$ is the slope at any position x.

$$EI\tan\theta = \frac{\tau}{2d}x^2 - \tau x + \frac{1}{3}\tau x_c \quad (1)$$

Depending on how the system is configured, including variations in the positioning of the base relative to the whisker, the choice of transducer, and any additional assumptions, it is possible to develop the model [48]. This model can then be used to assess the impact of an object's contour on the deflection signal patterns. After its first implementations [55, 58], variations of this approach have been studied extensively. Linearized solutions have been proposed in conjunction with sensor designs that allow simplifications of the ODE [36, 39, 91], but attempts have also been made to solve the ODE's numerically [57] and analytically [38, 92]. However, the elastica model relies on an assumption of a single point contact (SPC). For surfaces characterized by low curvature or minimal friction, this assumption becomes untenable as the shaft undergoes transverse sliding and contact force increases [91]. Illustrated in Figure 4B, this is known as lateral slip and poses a challenge in 3D contact point localization. Active [91] and passive [93] solutions exist to try and correct for lateral slip. The passive solution proposed by *Solomon and Hartmann* [93] includes estimating the friction coefficient between the whisker and the surface. By analysing the degradation in accuracy of the model under different friction conditions and object lateral curvatures, specific movement strategies can be selected to alleviate these inaccuracies. An extension of this research introduced the whisker-sweeping technique [39]. This novel sweeping method allows for continued estimation of contact point - all the while accounting for lateral slip. As such, we move away from probing/tapping, and are able to extract a continuous segment of an object's profile with a single whisk using torque information with sub-millimeter accuracy. *Will et al.* [92] expanded upon this method by including a single equation for a decision of the contact behaviour of the shaft with the object: contact at the tip, or contact between base and tip.

Limitations of using a physical model such as the elastica model for contact localization are that restrictions are imposed on the design and application. The method favours straight, cylindrical, uniform beams - imposing restrictions on sensor design. Many of the elastica solutions require bulky sensors, such as load cells, for accurate shape inference. This makes scalability and integration into a platform difficult. In addition, most literature assumes a convex-shaped environment with low curvature to ensure that the SPC condition is met. For concave objects, the SPC condition cannot always be met (Figure 4A). Recently, *Merker et al.* [59] proposed a method in which two-point-contacts (TPC) can be identified by analysing the kinks in support reactions produced at the base of the sensor.

With the limitations of a physical model in mind, *Lin et al.* [47] demonstrate the ability of three different Bayesian filtering algorithms (Extended Kalman Filter (EKF), Unscented Kalman Filet (UKF), and Particle Filter) [94] to outperform the novel sweeping algorithm [39] by achieving tracking within sub-millimeter accuracy (schematic of whisker design shown in Figure 3-I2). This accuracy is achieved without actuation (which previously outlined methods [95] require for accurate contact localization). Through use of a calibration set-up, the issue of non-unique bending moments (Figure 4C) to contact localization is mitigated by creating a data-driven sensor model (a mapping of contact point locations to predicted moment measurements). Along with a process model, the sensor model is fed to a Bayesian filter to find the probability distribution of the contact location. *Xiao et al.* [34] obtain the contact sequence through Hopf oscillator implementation and directly connect the contact points to extract object contours. In addition, a classification algorithm is implemented. The classification algorithm [1, 96] transforms contour points and probing points into higher dimensions using a multilayer perceptron (MLP) with ReLU activation function. To our knowledge, this is one of the only probabilistic object classification algorithms implemented for vibrissae-inspired sensors. Geometric object classification has been done previously by *Russel* [97], by fitting geometric primitives, and Bayesian filtering has been previously introduced in simulation [98]. As such, there remains a notable research gap in the broader exploration and development of probabilistic/data-driven techniques for addressing challenges in shape inference and contact point localization.

4.2 Navigation

Tactile sensing for navigation, as opposed to shape inference, is a less explored area due to the short range nature of the sensor and limited informative value for each contact (Figure 4D). Due to this, a large variation exists between the different approaches discussed in literature. However, research in this field has demonstrated the potential of whisker-inspired sensors for obstacle avoidance [31, 61, 64], wall/contour following [29, 31, 38], scene exploration [34] and SLAM [49]. Despite their short range, these sensors can repeatedly interact with their environment to make inferences whenever necessary, without damaging or changing the state of the environment. This would be more difficult with, for example, planar pushing [87].

Wall following and obstacle avoidance (often tackled hand-in-hand) are reactive navigational behaviours that are achievable using whisker-inspired sensors. Although a seemingly simple task, wall following behaviour can provide a basis for short-range SLAM solutions [99]. One of the simplest wall following methods would be to mount at least two neighbouring whiskers onto a platform and adjust the heading of the platform based on the difference in readings between the whiskers [31]. The schematic of the set-up required in

shown in Figure 3-M3. This navigation is purely reactive, and thus does not create an internal map, does not have memory, and does not learn. This initial reactive behaviour can thus be extended to *purposeful navigation*. Purposeful navigation includes the use of a *Purposive Map* (PM) [100]. The PM is a graph in which the nodes are representative of specific points in the environment that are to be sensed by the robot. Links in the graphs serve as indications of the robot behaviour that should be triggered in order to move to the following node. As such, the mobile robot is able to follow a predetermined path, while purposefully avoiding detected obstacles by selecting the desired behaviour from the PM. This navigation system is able to learn the environment by adding new nodes and links to the PM as additional landmarks are detected during its locomotion, and is reminiscent of current Simultaneous Localisation and Mapping (SLAM) solutions. Such 'desired behaviour' for obstacle avoidance was also implemented by *Fend et al.* [65] through Distributed Adaptive Control (DAC) [101, 102] by learning a set of hardwired reflexes based on readings from an infrared sensor. By repeated correlated activity in whisker sensors and infrared sensors, connections are formed such that the avoidance reflex can be triggered solely by activity in the whisker sensor.

More recently, the algorithms have moved towards active navigation through exploratory policy design [34] and SLAM [49]. Tactile exploration plays an essential role in accomplishing various objectives within robotics and machine perception, encompassing tasks like object identification, scene reconstruction, and the formulation of manipulation strategies [34]. Designing an exploration policy for a whisker-based agent is a challenge that hinges on the efficient sampling of information to gather sufficient data for subsequent control actions. Recently, *Xiao et al.* [34] implemented a hybrid exploration policy that switches between two states defined in a finite state machine (FSM): Object Searching (OS) and Contour Tracing (CT). The OS policy is an informative path planning (IPP) method [103, 104], based on an information acquisition function and an occupancy map. The information acquisition function is estimated through a Gaussian process with an RBF kernel. Within the search space, a rapidly-exploring random tree is expanded, and a heuristic sampling process guides the expansion towards regions with a high acquisition function value. From the fully expanded tree, the path that maximises the acquisition function is chosen. The policy for the CT state is a Hopf oscillator that is used to generate a path along the object contour. The FSM, inspired by the procedures that characterizes human exploration [105], switches from OS to CT when a contact event occurs. Exploration efficiency metrics showed that the policy performed well, and the agent was even able to choose and propagate through paths that were were planned through small areas of the environment. The main limitation of this system is the loss of accuracy in cluttered environments, as mapped objects begin to merge into each other. The mounted whisker sensor is shown in Figure 3-M1.

The primary goal of SLAM is to provide the ability for a robot to operate in an environment that is unknown, unstructured, and possibly dynamic, by continuously updating a map of the environment and its own location within it [106, 107]. Implementation of SLAM algorithms for tactile sensors has been done successfully with GPIS and pose estimation on a factor graph [87], and using particle filters [108]. Other SLAM solutions formulated for short-range sensors have been proposed in simulation [98, 99] are often designed to make probabilistic inferences about the environment based on hierarchical model priors, for example, identifying a table by sensing one leg. Implemented SLAM solutions for vibrissal sensors range from 2D [50, 51], to 3D [52], to 6D [49] solutions.

The 2D solutions both use standard particle filters. In [50], a simple FSM is implemented to determine control actions based on contact/no-contact with a whisker. Whereas in [51] the whisker sensory information is transformed into a 3D map that represents the volume surrounding the robot's head, allowing the robot to locate the most salient point in the environment. The robot's head and body are moved to direct its nose towards this point, while the whiskers are positioned mid-protraction to enhance exploration, wall following and novelty seeking behaviors [109]. The mapping aspect of tactile SLAM may be viewed as a lower resolution shape-inference problem as discussed in Subsection 4.1. Simple mapping may be achieved by fusing a small, local Gaussian distribution into the grid map at the contact location [50, 51]. To extend this, the assumption can be made that all objects in an environment are primarily made of long, straight edges. Thus, a blur of long, oriented edges are placed at the location of contact [50] based on the difference in contact angle between two whiskers. Data driven approaches may also be considered in which geometric templates are trained based on data collected by driving the robot into a wall at different angles multiple times [50, 110]. As expected, this template-based mapping achieved better contour predictions than the previous two methods [50]. However, it can only discriminate between trained contact points. Training the classifier on every possible contact would be impractical, reinforcing the point made in Subsection 4.1 that there may lie solutions in probabilistic methods [111, 112].

The 3D and 6D solutions are implementations of the existing vision-based SLAM algorithm: RatSLAM [113], for tactile data. In [52], tactile data is fed to RatSLAM in the form of tactile images. Tactile information is represented as a single point contact at the tip of the whisker. Each whisker is represented as a 3x6 pixel image. The intensity of each pixel is proportional to the estimated vertical height of an encountered object. This system was able to demonstrate loop closure [51]. The grid-based mapping approaches as proposed for the 2D solutions are limited in terms of the size and resolution of the map that can be created and updated

with constrained computing resources. The RatSLAM algorithm creates a topological map by associating local view and odometry, which are projected as nodes and edges into a 2D plane called the *experience map*. However, due to the limited sensory information available from the whisker-array and ambiguity in local views, there is a high potential for incorrect re-localization with RatSLAM [49]. Vibrissal sensing for SLAM presents an additional challenge due to the correspondence problem: in order to reduce uncertainties in pose estimation, the objects encountered during exploration must be uniquely discernible as known landmarks [49] (illustrated in Figure 4E). To address this issue, the RatSLAM algorithm has been extended to include explicit landmarks in the experience map [49]. This is achieved by introducing a mode switch triggered by the robot's interaction with the environment. When the robot encounters an object, the algorithm switches to *object exploration mode*, which initializes a new 6D map called an object exploration map. Similar to [34], this is a more elaborate shape inference algorithm [83], integrated into a global navigation algorithm in order to accomplish better mapping, localization and exploration capabilities. The whisker design used for this application can be seen in Figure 3-I3.

4.3 Texture Discrimination

Studies of texture discrimination in rats show the importance of so called 'stick-slip' events, which describes the continuous transition between static and dynamic contact with a surface. The application of texture discrimination in robotics is varied. For example, it may be beneficial for a household robot (such as a Roomba [115]) to be able to discriminate between textures when cleaning. Terrain exploration (and mapping) may be improved [36] with added texture information. Or, it may aid in estimating the error in odometry data on a mobile robot, such that localization can be improved [63]. Texture discrimination and classification has been done through temporal [54] and frequency [22] methods. Two main approaches exist: the first applies a Fourier Transform, the texture of the surface can be inferred from the Power Spectral Density (PSD) of the tactile data [22]. Alternatively, a feature based method [116] can be adopted in which a model is trained to differentiate between (and classify) textures based on a set of chosen features.

Qualitative texture discrimination can be achieved by transferring the whisker sensor data into the frequency domain [22]. From this, a human observer can distinguish the different spectra and infer which textures correspond to the spectra. Similarly, the power spectra of individual sweeps were computed, smoothed, and combined together to generate an average-power spectrum by *Fend et al* [60]. They concluded that texture identification could be improved by using all whiskers at the same time and by sweeping the whiskers across a surface multiple times. *Schultz et al. Schultz et al.* [36] presented spectra for five surfaces of three different types, through which smooth and rough textures were distinguishable by eye. However, no formal classification of textures was implemented. As illustrated in Figure 4F, the classification of textures through a frequency analysis poses a challenge. As accurate texture discrimination relies on the sensitivity of the whisker, we may also expect a lower SNR - making it challenging to achieve classification. Furthermore, the perceived signal is dependent on the characteristics of the whisker, which is difficult to encode into such a frequency analysis.

In contrast, *Seth et al* [29] presented a robot that used whisker-based sensing to explore a walled environment and learn to avoid textures associated with a negative reward. They analyzed the data in the time domain, with 20 lagged curvature inputs fed into a biologically inspired neural network classifier. *Kim and Möller* [46] also performed similar experiments using a non-actuated steel whisker attached to a fixed base contacting a rotating, textured drum. A neural network was used to classify the low-band spectra and achieved a success rate of 85% accurate classification over seven textures. However, classification was better with shorter whiskers and the classifier failed when the whisker base was allowed to move. Classification was also attempted by *Hipp et al.* [45], actuated whiskers were used to differentiate between eight different grades of sandpaper with a success rate of 39% using multidimensional Gaussian density estimators.

Quantitative classification of textures of an unconstrained base was introduced by *Fox et al.* [37] by providing useful statistics of data or 'features' as inputs to a standard classifier (Gaussian [117]). Several higher-level candidate features within and across three different experimental settings (the position and movement of the robot platform relative to the investigated surface) were tested. Frequency-based classifiers were able to perform well within a setting, but did not generalize particularly well across settings. The two best performing classifiers were based on the primary afferent model (PA) [70, 118] and on the onset feature. The onset feature is recognizable in rough surfaces as an increase in energy in the 2-3 kHz band, and acoustically by a pronounced 'click' sound when the whisker interacts with the surface [37]. The use of features was also shown by *Giguere et al.* [35], where 8 features were extracted from the sensor's (accelerometer) measurements in both the time and frequency domains. The neural network classifier, trained on a data-set of over ten different indoor and outdoor surfaces, was sensitive enough to discriminate between tiled and untiled linoleum. More recently, a state vector machine (SVM) model was implemented for texture discrimination and classification [38]. Four features of the signal were selected to be used for classification of four textures; the signal energy (ENG), spectral entropy (SEN), spectral centroid (SCE), and average interval of peaks (AIP). During classification, each of the four support vector matrices are convolved with the input vector. The matrix that

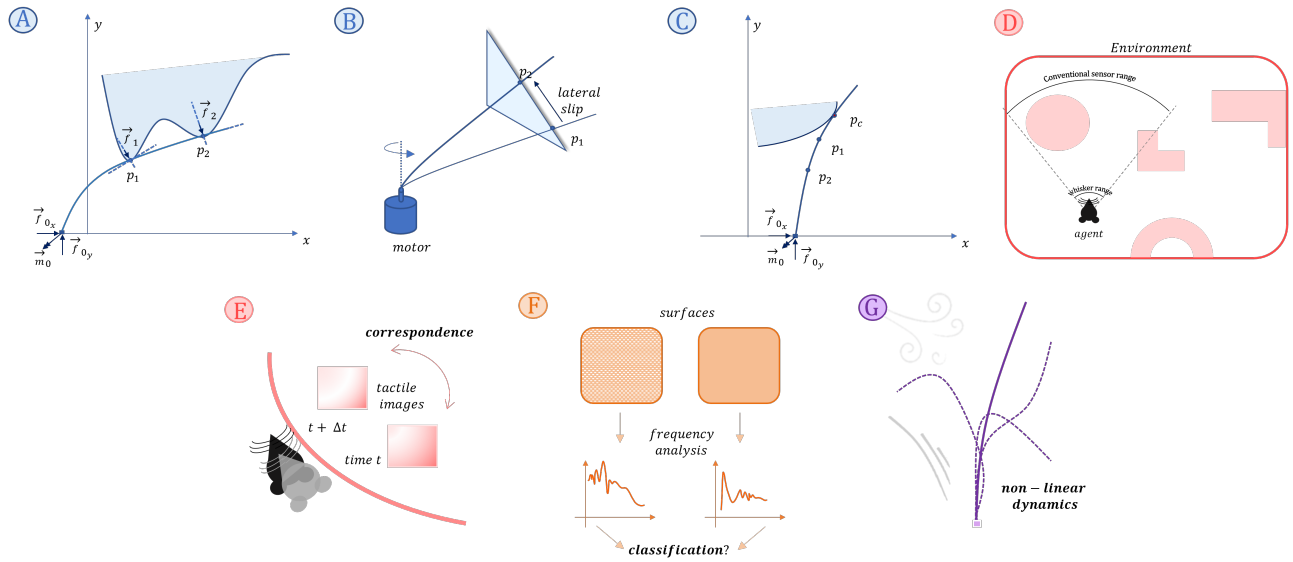

Figure 4 Challenges per robotic application. Colours correspond to applications as indicated in Figure 2. **—A:** Multi Point Contact. Solutions addressed in [59]. **—B:** Lateral Slip. Solutions addressed in [47, 91, 93]. **—C:** Non-unique mapping of contact location and bending moment. Solutions addressed in [47, 95]. **—D:** Short-range sensor. Solutions addressed in [34, 51, 98, 99]. **—E:** The correspondence problem. Solutions addressed in [49]. **—F:** Texture classification problem. Solutions addressed in [35, 37, 38]. **—G:** Non-linear/unknown shaft dynamics in turbulent flow conditions. Solutions addessed in [114].

results in highest convolution score indicates the texture. If all four scores are below 0.3, the model will output ”none”. The accuracy of this classifier was 88.3%, and has an advantage over neural network and Gaussian classifiers due to the lower amount of training data needed and computational time respectively. It must be noted, however, that the model was made to classify four varied textures (writing paper, flannelette, tissue paper, sandpaper). As such, no conclusions can be drawn on how successful this SVM model would work on, for example, different grades of sandpaper (as was attempted in [45]).

4.4 Fluid Profile Analysis

To our knowledge, fluid flow analysis is the most recent addition to vibrissal sensing applications. As we know, when an external load is applied to a whisker, the forces and moments are transmitted through the whisker shaft and result in the deformation of the ”follicle” (measured by a transducer). However, the external load is not limited to contact-only situations, but can also exist from fluid flow interactions around the whisker. With the first papers being published only around 2014, the amount of research done is limited. However, efforts have already been made to reconstruct tomographic images [44], map gas fields [69], investigate characteristic mechanical responses to airflow stimuli [114], and observe differences between airflow stimuli and inertial stimuli due to whisking [26]. While some inspiration is drawn from mammalian vibrissae such as rats, research also stems from marine mammals such as sea lions [27], whiskers located on bat wings [119], and on hair-like airflow sensors as found on arthropods [120–122]. As such, there is a strong foundation in nature to pursue whisker-inspired sensors as airflow sensors. From an engineering standpoint, the sensitivity can be easily controlled by choosing suitable materials, shapes, and transducers (see Table 1). This way, multi-modal sensors may be achieved that are suitable for both contact/no-contact detection. Applications range from collecting relative velocity information, to gust rejections [33], to obstacle avoidance. And in accordance with[33, 53], see large benefits for implementation on drones.

Solomon et al. [42] proposed an array of whisker-like sensors made of flexible plastic strips that were deflected by a stream of air flowing towards the center of the array. The deflection of each whisker provided an estimate of the flow velocity at a given height, but did not allow for the reconstruction of a full 2-D cross-sectional image of the fluid-flow field. *Takei et al.* [69] developed electronic whiskers based on highly tunable composite films of carbon nanotubes and silver nanoparticles patterned on high-aspect-ratio elastic fibers. The whiskers exhibited excellent bendability and high strain sensitivity, with a pressure sensitivity of up to approximately 8%/Pa. The authors demonstrated the ability to map 2D and 3D gas fields using these electronic whiskers. *Tuna et al.* [44] proposed a novel tactile fluid flow imaging technique that relates rat’s whisker movements to tomographic imaging to extract fluid-flow characteristics with a robotic whisker array (set-up shown in Figure 3-M4). The experimental re-

sults demonstrated that the approach offers a fundamentally novel sensor technology for flow-field measurements. However, relative errors between 19-45% were reached when testing three different steady flow patterns.

Evidently, one of the challenges of using vibrissal sensors for fluid profile sensing is that the dynamics of the whisker must be known in order to be able to make inferences of the fluid field with which the system is interacting. This challenge is illustrated in Figure 4G. *Yu et al.* [114] investigated the mechanical response of isolated rat macrovibrissae to airflow. The following main conclusions are drawn:

1. The whisker bends primarily in the direction of airflow and vibrates around a new average position at frequencies related to its resonant modes
2. The bending direction is not affected by airflow speed or by geometric properties of the whisker
3. The bending magnitude increases strongly with airflow speed and with the ratio of the whisker's arc length to base diameter
4. To a much smaller degree, the bending magnitude also varies with the orientation of the whisker's intrinsic curvature relative to the direction of airflow.

Yang et al. [67] experimented with whisker's response to airspeed, showing that voltage readings appeared to be related to the adjustments in airspeed (consistent with the third conclusion by *Yu et al.* [114]). Characterisation of the whisker dynamics can also be attempted by means of vision-based methods (see Table 1). Cameras have been used to capture whisker dynamics under Von-Karman vortices to improve characterisation [27]. *Muthuramalingam et al.* provided a theoretical and experimental insight into the mechanism behind the detection of the Strouhal frequency of flow-induced oscillations of the whiskers. The authors proposed that the frequency response of the whiskers may be tunable by changing the material and geometric properties of the whiskers.

More recently, *Deer and Pounds* [33] use airflow sensing as a mechanism to detect the "bow-wave" of air pushed ahead of an approaching object in addition to fluid velocity sensing (shown in Figure 3-I1). The sensors are able to measure contact forces as low as 3.33 μN, and fluid velocities as high as 7.5 m/s. As the sensor is highly sensitive, it enables the detection of an approaching object's advancing pressure wave and can thus aid in anticipating impending contacts. A warning of 0.037 seconds can be given for a hand moving at 0.53 m/s when it is 20 mm away and detected by the system. To our knowledge, this is the first insight into using the whiskers as airflow sensors to aid in decision making. It does beg the question of how robust this application may be to false positives - as a suitable pressure threshold needs to be found that eliminates detections due to inertial motion of the platform. However, this development could make for very interesting obstacle detection systems. Especially for aerial robotics, where such "bow waves" may be more apparent pre-contact. Most notable is that the same whisker array is used for both contact and pre-contact modalities, with good results. While multi-modal biomimetic vibrissal sensors have started arising, the ability to distinguish the type of modality during signal processing poses a challenge.

One of the advantages of whisker-inspired sensors is their ability to detect fluid flows with high sensitivity and resolution, even in low-speed and turbulent environments. Additionally, by using insights from hair-like sensors on arthropods, miniaturisation is achievable, allowing for the creation of small and precise sensors. *Dagamseh et al.* [120] developed this concept by fabricating an artificial hair flow-sensor using MEMS surface micro-machined technology. The sensor consists of a suspended silicon nitride membrane with a 1 mm long SU-8 hair on top. By extending the sensor to an array formation [121] with separate electrodes, the measurement of signals from different hairs individually and simultaneously are taken. A Frequency Division Multiplexing (FDM) technique was used as an array-addressing scheme to reduce the complexity of interfacing hair-sensor arrays. Furthermore, an additional advantage of using whisker-inspired sensors as airflow sensors is that directionality can be achieved if the transducers are implemented appropriately.

Greater sensitivity also gives way to lower signal to noise ratios (SNR). Most studies thus far consider airflow experiments in very controlled environments. As such, generalized conclusions, other than those presented in [114], can not yet be drawn across all environments. Whisker dynamics in turbulent environments may be difficult to characterise, meaning that effective signal processing can become challenging (Figure 4G). A notable trend that is observable in [42, 44, 53] is the modification of the whisker sensors with flatter, large pieces of plastic such that the surface area normal to the flow is increased. This modification also aids in increasing SNR.

5 Challenges and Opportunities

Most research thus far focuses either on experimentation with isolated whisker-inspired sensors, or mounts the sensors on a mobile platform. Very little work has been done thus far on underwater or aerial applications. Especially underwater, evidence suggests that harbour seals are able to discriminate object shape and location based on the produced wakes [9]. This presents intriguing opportunities for additional sensory capacity for autonomous underwater vehicles (AUV). For aerial applications, opportunities exist for search and rescue missions and 3D mapping of locations such as caves or other hard-to-reach environments. Although drones add complexity due to the added degrees of freedom, the easy maneuverability may be beneficial for passive whisking purposes. As such, sensor complexity may be reduced.

Vibrissae found in nature are multi-modal, meaning they are able to perform all four of the above mentioned tasks si-

multaneously. Next to the challenges outlined per application (illustrated in Figure 4), the most over-arching problem is that we are not yet able to achieve the same modality that is found in nature. Recently, some multi-modal sensors have been developed [33, 34]. However, the application is known during the performed experiments. As such, it is still unclear how one could clearly distinguish which whisker motions/behaviours belong to which stimuli [26]. This is especially the case when considering the combinations of whisking, airflow and contact signals. *Kent et al.* [26] performed experiments using a vision-based set-up to try and classify stimuli by the associated signals. Whiskers were subjected to high, medium, and low airflow speeds. Deliberately, no attempt was made to ensure laminar airflow such that the airflow was more comparable to the natural environment. The inertial effects introduced by whisking [123, 124] can be distinguished from the effects of airflow by their frequency content. The following main conclusions are drawn:

1. Non-contact mechanical stimuli like airflow and inertial forces tend to impact all whiskers in an array similarly, whereas contact stimuli can lead to more selective or localized responses.

2. Compared to the higher frequency oscillations that accompany airflow, inertial motion leads to relatively smoother and lower frequency translations of the whisker.

While these conclusions provide valuable insights into dynamic behaviour of whisker arrays; a standardized whisker shaft design is currently lacking, making characterisation of whisker behaviour difficult. Understanding and predicting sensor response to stimuli is imperative to advance signal processing capability across all modalities.

In addition, scalability remains a challenge. As previously discussed, arrays are required to aid in data acquisition. If multi-modality is to be achieved, each whisker needs to have an appropriate transduction mechanism to account for all stimuli. In our opinion, the most promising transducer currently is the MEMS barometer; lightweight, accurate, and has already demonstrated multi-modal applications [33]. However, achieving similar modalities and accuracy to biological whiskers would require a significant increase in computational and hardware complexity [26].

From these challenges, one of the greatest opportunities that we identify is to use probabilistic and data-driven methods to aid in characterising the whisker sensor, and in the tasks to be performed. A great example of where this was successful was in [47], where Bayesian filtering and a data-driven calibration set-up was used to achieve high-accuracy contact localization along the whisker in the presence of slip. Compared to image-based sensors, for example, there is much more freedom to place the sensor on a platform. And due to the light-weight structure, ease of manufacturing, and low RAM/CPU requirements for the additional data, not many hurdles are faced when we want to extend the sensory capacity with these sensors. As such, we could have access to data in locations in which we would otherwise not easily be able to place other sensors. By exploiting this opportunity, and by applying more probabilistic and data driven methods, we believe there is potential to bring this novel sensing technology to higher accuracy results and increased modality.

6 Conclusion

This literature review presented past and current work in the domain of vibrissal sensing for robotic applications. Four general applications/taxonomies were identified: *shape inference, navigation, texture discrimination* and *fluid flow*. Physical design choices were discussed, and the implemented algorithms in literature were outlined across all four applications. It has been shown that, regardless of the challenges faced, vibrissal sensing proves to be a promising tactile sensing method to improve the sensory capacity of robots. As the rodent's vibrissal system remains a common model for investigating the mechanisms of sensorimotor integration and active sensing [4, 5], we believe that there exists the unique opportunity to continuously improve upon robotic sensing from both the physical sensor design, as well as the signal processing methods congruently. By closely aligning the biological and robotic modalities, multi-modal sensing for robotics using whisker-inspired sensors may allow for a wide range of sensing capabilities that have not yet been realized by traditional sensors.

7 Further Research

The challenges and opportunities discussed in Section 5 highlight a clear research gap in the area of whisker-based tactile navigation for aerial robotics. As such, the follow-up research to this literature review will be a preliminary whisker-based tactile navigation solution for drones. The research will use a SpeedyBee frame [125] with a PixRacer R15 autopilot [126]. The MAV will be equipped with 16 whisker-inspired sensors. Each sensor comprises a 200mm nitinol wire (diameter: 0.4 mm) attached to a follicle structure made up of three MEMS barometers and an integrated microcontroller PCB. The follicle is attached to the whisker shaft by means of a UV resin, creating a so called "follicle structure sensing unit". As a first step, these 16 modular whisker-inspired sensors will be mounted onto the SpeedyBee frame to perform contour following and obstacle avoidance tasks. We believe that by addressing contour following as the first navigational task, we also address challenges associated with shape inference (and if time permits, texture discrimination). Furthermore, as the sensors are to be mounted onto an aerial platform, we expect to encounter more challenges stemming from inertial movements and vibrations when compared to a mobile platform. As such, we believe this research to provide a foundation for future whisker-based tactile SLAM solutions

for aerial platforms. The following main research question will be addressed:

To what extent can a drone equipped with our 16 modular whisker-inspired sensors achieve accurate contour following, measured by its ability to maintain a desired distance from contours of varying curvature?

In answering this research question, the following sub-questions will be extensively explored:

A **Metric Definition:**

- i How can accuracy in contour following be precisely defined in the context of maintaining a desired distance from a contour?

B **Methodology:**

- i How does the drone's performance vary when following contours with different curvatures?
- ii What are the key indicators of successful contour following, including wall contact identification, orientation inference, sustained contact, and consistent distance maintenance?

C **Literature Comparison:**

- i How does the performance of the whisker-inspired sensor-equipped drone compare to the simple implementation by Jung & Zelinsky (1996) [31]?
- ii How does the performance of our suggested drone solution compare to the complex contour-following solutions presented by Zhang et al. (2022) [38] and Xiao et al. (2022) [34], considering factors such as accuracy, robustness, and adaptability to varying environmental conditions?

D **Challenges and Solutions:**

- i What are the primary challenges associated with mounting whisker-inspired sensors onto an MAV, considering factors such as vibrations, inertial effects, and interaction with propeller wake?
- ii How can these challenges be addressed to ensure accurate and reliable contour following in a real-world environment?

E **Applications:**

- i What specific advantages does accurate contour following by the drone offer for search and rescue missions in environments with limited visibility, such as dark or smoke-filled areas?
- ii How could the drone's contour-following capabilities be applied to navigate and explore confined spaces, such as caves, that are challenging for human access?

By addressing these sub-questions, our research will comprehensively investigate the feasibility, challenges, and potential applications of using whisker-inspired sensors for contour following by drones.

REFERENCES

[1] Shan Luo, Joao Bimbo, Ravinder Dahiya, and Hongbin Liu. Robotic tactile perception of object properties: A review. *Mechatronics*, 48: 54–67, December 2017. ISSN 0957-4158. doi: 10.1016/j.mechatronics.2017.11.002. URL https://www.sciencedirect.com/science/article/pii/S0957415817301575.

[2] Mohamad-Ammar Sayegh, Hammam Daraghma, Samir Mekid, and Salem Bashmal. Review of Recent Bio-Inspired Design and Manufacturing of Whisker Tactile Sensors. *Sensors*, 22, April 2022. doi: 10.3390/s22072705.

[3] Mathew E. Diamond, Moritz von Heimendahl, Per Magne Knutsen, David Kleinfeld, and Ehud Ahissar. 'Where' and 'what' in the whisker sensorimotor system. *Nature Reviews. Neuroscience*, 9 (8):601–612, August 2008. ISSN 1471-0048. doi: 10.1038/nrn2411.

[4] S.B. Vincent. The function of the vibrissae in the behavior of the white rat. *Animal Behavior Monographs*, 1, 5:84–84, 1912.

[5] W. I. Welker. Analysis of Sniffing of the Albino Rat. *Behaviour*, 22(3/4):223–244, 1964. ISSN 0005-7959. URL https://www.jstor.org/stable/4533073. Publisher: Brill.

[6] Tony J. Prescott, Martin J. Pearson, Ben Mitchinson, J.C. W. Sullivan, and Anthony G. Pipe. Whisking with robots. *IEEE Robotics & Automation Magazine*, 16 (3):42–50, September 2009. ISSN 1558-223X. doi: 10.1109/MRA.2009.933624. Conference Name: IEEE Robotics & Automation Magazine.

[7] R. Blythe Towal, Brian W. Quist, Venkatesh Gopal, Joseph H. Solomon, and Mitra J. Z. Hartmann. The morphology of the rat vibrissal array: a model for quantifying spatiotemporal patterns of whisker-object contact. *PLoS computational biology*, 7(4):e1001120, April 2011. ISSN 1553-7358. doi: 10.1371/journal.pcbi.1001120.

[8] J. Dörfl. The musculature of the mystacial vibrissae of the white mouse. *Journal of Anatomy*, 135(Pt 1): 147–154, August 1982. ISSN 0021-8782.

[9] Sven Wieskotten, Björn Mauck, Lars Miersch, Guido Dehnhardt, and Wolf Hanke. Hydrodynamic discrimination of wakes caused by objects of different size or shape in a harbour seal (Phoca vitulina). *The Journal of experimental biology*, 214:1922–30, June 2011. doi: 10.1242/jeb.053926.

[10] Marcin Szwed, Knarik Bagdasarian, Barak Blumenfeld, Omri Barak, Dori Derdikman, and Ehud Ahissar. Responses of trigeminal ganglion neurons to the radial distance of contact during active vibrissal touch. *Journal of Neurophysiology*, 95(2):791–802, February 2006. ISSN 0022-3077. doi: 10.1152/jn.00571.2005.

[11] Per Magne Knutsen and Ehud Ahissar. Orthogonal coding of object location. *Trends in Neurosciences*, 32(2):101–109, February 2009. ISSN 0166-2236. doi: 10.1016/j.tins.2008.10.002.

[12] J. Alexander Birdwell, Joseph H. Solomon, Montakan Thajchayapong, Michael A. Taylor, Matthew Cheely, R. Blythe Towal, Jorg Conradt, and Mitra J. Z. Hartmann. Biomechanical models for radial distance determination by the rat vibrissal system. *Journal of Neurophysiology*, 98(4):2439–2455, October 2007. ISSN 0022-3077. doi: 10.1152/jn.00707.2006.

[13] D. J. Krupa, M. S. Matell, A. J. Brisben, L. M. Oliveira, and M. A. Nicolelis. Behavioral properties of the trigeminal somatosensory system in rats performing whisker-dependent tactile discriminations. *The Journal of Neuroscience: The Official Journal of the Society for Neuroscience*, 21(15):5752–5763, August 2001. ISSN 1529-2401. doi: 10.1523/JNEUROSCI.21-15-05752.2001.

[14] M. A. Harvey, R. Bermejo, and H. P. Zeigler. Discriminative whisking in the head-fixed rat: optoelectronic monitoring during tactile detection and discrimination tasks. *Somatosensory & Motor Research*, 18 (3):211–222, 2001. ISSN 0899-0220. doi: 10.1080/01421590120072204.

[15] E. Guić-Robles, C. Valdivieso, and G. Guajardo. Rats can learn a roughness discrimination using only their vibrissal system. *Behavioural Brain Research*, 31(3):285–289, January 1989. ISSN 01664328. doi: 10.1016/0166-4328(89)90011-9. URL https://linkinghub.elsevier.com/retrieve/pii/0166432889900119.

[16] G. E. Carvell and D. J. Simons. Biometric analyses of vibrissal tactile discrimination in the rat. *The Journal of Neuroscience: The Official Journal of the Society for Neuroscience*, 10(8):2638–2648, August 1990. ISSN 0270-6474. doi: 10.1523/JNEUROSCI.10-08-02638.1990.

[17] Daniel B. Polley, Jessica L. Rickert, and Ron D. Frostig. Whisker-based discrimination of object orientation determined with a rapid training paradigm. *Neurobiology of Learning and Memory*, 83(2):134–142, March 2005. ISSN 1074-7427. doi: 10.1016/j.nlm.2004.10.005. URL https:

//www.sciencedirect.com/science/article/pii/S1074742704001212.

[18] Carl C. H. Petersen. The functional organization of the barrel cortex. *Neuron*, 56(2):339–355, October 2007. ISSN 0896-6273. doi: 10.1016/j.neuron.2007.09.017.

[19] R. Blythe Towal and Mitra J. Hartmann. Right–Left Asymmetries in the Whisking Behavior of Rats Anticipate Head Movements. *Journal of Neuroscience*, 26(34):8838–8846, August 2006. ISSN 0270-6474, 1529-2401. doi: 10.1523/JNEUROSCI.0581-06.2006. URL https://www.jneurosci.org/content/26/34/8838. Publisher: Society for Neuroscience Section: Articles.

[20] Robyn Grant, Ben Mitchinson, Charles Fox, and Tony Prescott. Active Touch Sensing in the Rat: Anticipatory and Regulatory Control of Whisker Movements During Surface Exploration. *Journal of neurophysiology*, 101:862–74, December 2008. doi: 10.1152/jn.90783.2008.

[21] Puhong Gao, Roberto Bermejo, and H. Philip Zeigler. Whisker Deafferentation and Rodent Whisking Patterns: Behavioral Evidence for a Central Pattern Generator. *Journal of Neuroscience*, 21(14):5374–5380, July 2001. ISSN 0270-6474, 1529-2401. doi: 10.1523/JNEUROSCI.21-14-05374.2001. URL https://www.jneurosci.org/content/21/14/5374. Publisher: Society for Neuroscience Section: ARTICLE.

[22] M. Lungarella, V.V. Hafner, R. Pfeifer, and H. Yokoi. An artificial whisker sensor for robotics. In *IEEE/RSJ International Conference on Intelligent Robots and Systems*, volume 3, pages 2931–2936 vol.3, September 2002. doi: 10.1109/IRDS.2002.1041717.

[23] Christopher M. Williams and Eric M. Kramer. The Advantages of a Tapered Whisker. *PLOS ONE*, 5(1):e8806, January 2010. ISSN 1932-6203. doi: 10.1371/journal.pone.0008806. URL https://journals.plos.org/plosone/article?id=10.1371/journal.pone.0008806. Publisher: Public Library of Science.

[24] Mitra J. Hartmann, Nicholas J. Johnson, R. Blythe Towal, and Christopher Assad. Mechanical Characteristics of Rat Vibrissae: Resonant Frequencies and Damping in Isolated Whiskers and in the Awake Behaving Animal. *Journal of Neuroscience*, 23(16):6510–6519, July 2003. ISSN 0270-6474, 1529-2401. doi: 10.1523/JNEUROSCI.23-16-06510.2003. URL https://www.jneurosci.org/content/23/16/6510. Publisher: Society for Neuroscience Section: Behavioral/Systems/Cognitive.

[25] Hayley M. Belli, Anne E. T. Yang, Chris S. Bresee, and Mitra J. Z. Hartmann. Variations in vibrissal geometry across the rat mystacial pad: base diameter, medulla, and taper. *Journal of Neurophysiology*, 117(4):1807–1820, April 2017. ISSN 0022-3077. doi: 10.1152/jn.00054.2016. URL https://journals.physiology.org/doi/full/10.1152/jn.00054.2016. Publisher: American Physiological Society.

[26] Teresa A Kent, Suhan Kim, Gabriel Kornilowicz, Wenzhen Yuan, Mitra J. Z. Hartmann, and Sarah Bergbreiter. WhiskSight: A Reconfigurable, Vision-Based, Optical Whisker Sensing Array for Simultaneous Contact, Airflow, and Inertia Stimulus Detection. *IEEE Robotics and Automation Letters*, 6(2):3357–3364, April 2021. ISSN 2377-3766. doi: 10.1109/LRA.2021.3062816. Conference Name: IEEE Robotics and Automation Letters.

[27] Muthukumar Muthuramalingam and Christoph Bruecker. Seal and Sea lion Whiskers Detect Slips of Vortices Similar as Rats Sense Textures. *Scientific Reports*, 9(1):12808, September 2019. ISSN 2045-2322. doi: 10.1038/s41598-019-49243-5. URL https://www.nature.com/articles/s41598-019-49243-5. Number: 1 Publisher: Nature Publishing Group.

[28] Leiv Andresen, Emanuele Aucone, and Stefano Mintchev. Whisker-based Haptic Perception System for Branch Detection in Dense Vegetation. In *2022 IEEE 5th International Conference on Soft Robotics (RoboSoft)*, pages 911–918, April 2022. doi: 10.1109/RoboSoft54090.2022.9762143.

[29] A.K. Seth, J.L. McKinstry, G.M. Edelman, and J.L. Krichmar. Texture discrimination by an autonomous mobile brain-based device with whiskers. In *IEEE International Conference on Robotics and Automation, 2004. Proceedings. ICRA '04. 2004*, volume 5, pages 4925–4930 Vol.5, April 2004. doi: 10.1109/ROBOT.2004.1302498. ISSN: 1050-4729.

[30] Thomas Schlegl, Torsten Kröger, Andre Gaschler, Oussama Khatib, and Hubert Zangl. Virtual whiskers — Highly responsive robot collision avoidance. In *2013 IEEE/RSJ International Conference on Intelligent Robots and Systems*, pages 5373–5379, November 2013. doi: 10.1109/IROS.2013.6697134. ISSN: 2153-0866.

[31] D. Jung and A. Zelinsky. Whisker based mobile robot navigation. In *Proceedings of IEEE/RSJ International Conference on Intelligent Robots and Systems. IROS '96*, volume 2, pages 497–504 vol.2, November 1996. doi: 10.1109/IROS.1996.570842.

[32] R.A. Russell. Using tactile whiskers to measure surface contours. In *Proceedings 1992 IEEE International Conference on Robotics and Automation*, pages 1295–1299 vol.2, May 1992. doi: 10.1109/ROBOT.1992.220070.

[33] William Deer and Pauline E. I. Pounds. Lightweight Whiskers for Contact, Pre-Contact, and Fluid Velocity Sensing. *IEEE Robotics and Automation Letters*, 4(2):1978–1984, April 2019. ISSN 2377-3766. doi: 10.1109/LRA.2019.2899215. Conference Name: IEEE Robotics and Automation Letters.

[34] Chenxi Xiao, Shujia Xu, Wenzhuo Wu, and Juan Wachs. Active Multiobject Exploration and Recognition via Tactile Whiskers. *IEEE Transactions on Robotics*, 38(6):3479–3497, December 2022. ISSN 1941-0468. doi: 10.1109/TRO.2022.3182487. Conference Name: IEEE Transactions on Robotics.

[35] Philippe Giguere and Gregory Dudek. A Simple Tactile Probe for Surface Identification by Mobile Robots. *IEEE Transactions on Robotics*, 27(3):534–544, June 2011. ISSN 1941-0468. doi: 10.1109/TRO.2011.2119910. Conference Name: IEEE Transactions on Robotics.

[36] A.E. Schultz, J.H. Solomon, M.A. Peshkin, and M.J. Hartmann. Multifunctional Whisker Arrays for Distance Detection, Terrain Mapping, and Object Feature Extraction. In *Proceedings of the 2005 IEEE International Conference on Robotics and Automation*, pages 2588–2593, April 2005. doi: 10.1109/ROBOT.2005.1570503. ISSN: 1050-4729.

[37] Charles Fox, Ben Mitchinson, Martin Pearson, Anthony Pipe, and Tony Prescott. Contact type dependency of texture classification in a whiskered mobile robot. *Autonomous Robots*, 26:223–239, May 2009. doi: 10.1007/s10514-009-9109-z.

[38] Yulai Zhang, Shurui Yan, Zihou Wei, Xuechao Chen, Toshio Fukuda, and Qing Shi. A Small-Scale, Rat-Inspired Whisker Sensor for the Perception of a Biomimetic Robot: Design, Fabrication, Modeling, and Experimental Characterization. *IEEE Robotics & Automation Magazine*, 29(4):115–126, December 2022. ISSN 1558-223X. doi: 10.1109/MRA.2022.3182870. Conference Name: IEEE Robotics & Automation Magazine.

[39] Joseph Solomon and Mitra Hartmann. Extracting Object Contours with the Sweep of a Robotic Whisker Using Torque Information. *I. J. Robotic Res.*, 29:1233–1245, August 2010. doi: 10.1177/0278364908104468.

[40] Hannah Emnett, Matthew Graff, and Mitra Hartmann. A Novel Whisker Sensor Used for 3D Contact Point Determination and Contour Extraction. June 2018. doi: 10.15607/RSS.2018.XIV.059.

[41] James F. Wilson and Zhenhai Chen. A Whisker Probe System for Shape Perception of Solids. *Journal of Dynamic Systems, Measurement, and Control*, 117(1):104–108, March 1995. ISSN 0022-0434. doi: 10.1115/1.2798514. URL https://doi.org/10.1115/1.2798514.

[42] Joseph H. Solomon and Mitra J. Hartmann. Robotic whiskers used to sense features. *Nature*, 443(7111):525–525, October 2006. ISSN 1476-4687. doi: 10.1038/443525a. URL https://www.nature.com/articles/443525a. Number: 7111 Publisher: Nature Publishing Group.

[43] David Collinson, Hannah Emnett, Jinqiang Ning, and Mitra Hartmann. Tapered Polymer Whiskers to Enable Three-Dimensional Tactile Feature Extraction. *Soft Robotics*, 8, June 2020. doi: 10.1089/soro.2019.0055.

[44] Cagdas Tuna, Douglas L. Jones, and Farzad Kamalabadi. Tactile tomographic fluid-flow imaging with a robotic whisker array. In *2014 IEEE International Conference on Acoustics, Speech and Signal Processing (ICASSP)*, pages 6815–6819, May 2014. doi: 10.1109/ICASSP.2014.6854920. ISSN: 2379-190X.

[45] Joerg Hipp, Ehsan Arabzadeh, Erik Zorzin, Jorg Conradt, Christoph Kayser, Mathew E. Diamond, and Peter König. Texture Signals in Whisker Vibrations. *Journal of Neurophysiology*, 95(3):1792–1799, March 2006. ISSN 0022-3077. doi: 10.1152/jn.01104.2005. URL https://journals.physiology.org/doi/full/10.1152/jn.01104.2005. Publisher: American Physiological Society.

[46] Stefan Schaal, Auke Jan Ijspeert, Aude Billard, Sethu Vijayakumar, and Jean-Arcady Meyer. A biomimetic whisker for texture discrimination and distance estimation. In *From animals to animats 8: Proceedings of the Eighth International Conference on the Simulation of Adaptive Behavior*, pages 140–149. MIT Press, 2004. ISBN 978-0-262-29144-6. URL https://ieeexplore.ieee.org/document/6282101. Conference Name: From animals to animats 8: Proceedings of the Eighth International Conference on the Simulation of Adaptive Behavior.

[47] Michael Lin, Emilio Reyes, Jeannette Bohg, and Mark Cutkosky. *Whisker-Inspired Tactile Sensing for Contact Localization on Robot Manipulators*. October 2022. doi: 10.48550/arXiv.2210.12387.

[48] DaeEun Kim and Ralf Möller. Biomimetic whiskers for shape recognition. *Robotics and Autonomous Systems*, 55(3):229–243, March 2007. ISSN 0921-8890. doi: 10.1016/j.robot.2006.08.001. URL https://www.sciencedirect.com/science/article/pii/S0921889006001400.

[49] Mohammed Salman and Martin J. Pearson. Whisker-RatSLAM Applied to 6D Object Identification and Spatial Localisation. In Vasiliki Vouloutsi, José Halloy, Anna Mura, Michael Mangan, Nathan Lepora, Tony J. Prescott, and Paul F.M.J. Verschure, editors, *Biomimetic and Biohybrid Systems*, Lecture Notes in Computer Science, pages 403–414, Cham, 2018. Springer International Publishing. ISBN 978-3-319-95972-6. doi: 10.1007/978-3-319-95972-6_44.

[50] Charles Fox, Mat Evans, Martin Pearson, and Tony Prescott. Tactile SLAM with a biomimetic whiskered robot. In *2012 IEEE International Conference on Robotics and Automation*, pages 4925–4930, St Paul, MN, USA, May 2012. IEEE. ISBN 978-1-4673-1405-3 978-1-4673-1403-9 978-1-4673-1578-4 978-1-4673-1404-6. doi: 10.1109/ICRA.2012.6224813. URL http://ieeexplore.ieee.org/document/6224813/.

[51] Martin J. Pearson, Charles Fox, J. Charles Sullivan, Tony J. Prescott, Tony Pipe, and Ben Mitchinson. Simultaneous localisation and mapping on a multi-degree of freedom biomimetic whiskered robot. In *2013 IEEE International Conference on Robotics and Automation*, pages 586–592, May 2013. doi: 10.1109/ICRA.2013.6630633. ISSN: 1050-4729.

[52] Mohammed Salman and Martin J. Pearson. Advancing whisker based navigation through the implementation of Bio-Inspired whisking strategies. In *2016 IEEE International Conference on Robotics and Biomimetics (ROBIO)*, pages 767–773, December 2016. doi: 10.1109/ROBIO.2016.7866416.

[53] Suhan Kim, Regan Kubicek, Aleix Paris, Andrea Tagliabue, Jonathan P. How, and Sarah Bergbreiter. A Whisker-inspired Fin Sensor for Multi-directional Airflow Sensing. In *2020 IEEE/RSJ International Conference on Intelligent Robots and Systems (IROS)*, pages 1330–1337, October 2020. doi: 10.1109/IROS45743.2020.9341723. ISSN: 2153-0866.

[54] Moritz Scharff, Alencastre Jorge, and Carsten Behn. Detection of Surface Texture with an Artificial Tactile Sensor. In *Mechanisms and Machine Science*, pages 43–50. January 2019. ISBN 978-3-030-16422-5. doi: 10.1007/978-3-030-16423-2_4. Journal Abbreviation: Mechanisms and Machine Science.

[55] G.R. Scholz and C.D. Rahn. Profile sensing with an actuated whisker. *IEEE Transactions on Robotics and Automation*, 20(1):124–127, February 2004. ISSN 2374-958X. doi: 10.1109/TRA.2003.820864. Conference Name: IEEE Transactions on Robotics and Automation.

[56] Lukas Merker, Joachim Steigenberger, Rafael Marangoni, and Carsten Behn. A Vibrissa-Inspired Highly Flexible Tactile Sensor: Scanning 3D Object Surfaces Providing Tactile Images. *Sensors (Basel, Switzerland)*, 21(5):1572, February 2021. ISSN 1424-8220. doi: 10.3390/s21051572.

[57] T.N. Clements and C.D. Rahn. Three-dimensional contact imaging with an actuated whisker. *IEEE Transactions on Robotics*, 22(4):844–848, August 2006. ISSN 1941-0468. doi: 10.1109/TRO.2006.878950. Conference Name: IEEE Transactions on Robotics.

[58] T. Tsujimura and T. Yabuta. Object detection by tactile sensing method employing force/torque information. *IEEE Transactions on Robotics and Automation*, 5(4):444–450, August 1989. ISSN 2374-958X. doi: 10.1109/70.88059. Conference Name: IEEE Transactions on Robotics and Automation.

[59] Lukas Merker, Juan Fischer Calderon, Moritz Scharff, Alencastre Jorge, and Carsten Behn. Effects of Multi-Point Contacts during Object Contour Scanning Using a Biologically-Inspired Tactile Sensor. *Sensors*, 20:2077, April 2020. doi: 10.3390/s20072077.

[60] M. Fend, S. Bovet, H. Yokoi, and R. Pfeifer. An active artificial whisker array for texture discrimination. In *Proceedings 2003 IEEE/RSJ International Conference on Intelligent Robots and Systems (IROS 2003) (Cat. No.03CH37453)*, volume 2, pages 1044–1049 vol.2, October 2003. doi: 10.1109/IROS.2003.1248782.

[61] Hiroshi Yokoi, Max Lungarella, Miriam Fend, and Rolf Pfeifer. Artificial Whiskers: Structural Characterization and Implications for Adaptive Robots. *Journal of Robotics and Mechatronics*, 17(5):584–595, October 2005. doi: 10.20965/jrm.2005.p0584. URL https://www.fujipress.jp/jrm/rb/robot001700050584/. Publisher: Fuji Technology Press Ltd.

[62] Miriam Fend. Whisker-Based Texture Discrimination on a Mobile Robot. pages 302–311, September 2005. ISBN 978-3-540-28848-0. doi: 10.1007/11553090_31.

[63] N. Roy, G. Dudek, and P. Freedman. Surface sensing and classification for efficient mobile robot navigation. In *Proceedings of IEEE International Conference on*

Robotics and Automation, volume 2, pages 1224–1228 vol.2, April 1996. doi: 10.1109/ROBOT.1996.506874. ISSN: 1050-4729.

[64] Miriam Fend, Hiroshi Yokoi, and Rolf Pfeifer. Optimal Morphology of a Biologically-Inspired Whisker Array on an Obstacle-Avoiding Robot. June 2003. ISBN 978-3-540-20057-4. doi: 10.1007/978-3-540-39432-7_83.

[65] Miriam Fend, Simon Bovet, and Rolf Pfeifer. On the influence of morphology of tactile sensors for behavior and control. *Robotics and Autonomous Systems*, 54(8):686–695, August 2006. ISSN 0921-8890. doi: 10.1016/j.robot.2006.02.014. URL https://www.sciencedirect.com/science/article/pii/S0921889006000674.

[66] M. Kaneko, N. Nanayama, and T. Tsuji. Vision-based active sensor using a flexible beam. *IEEE/ASME Transactions on Mechatronics*, 6(1):7–16, March 2001. ISSN 1941-014X. doi: 10.1109/3516.914386. Conference Name: IEEE/ASME Transactions on Mechatronics.

[67] Anne En-Tzu Yang, Mitra J. Z. Hartmann, and Sarah Bergbreiter. Contact-Resistive Sensing of Touch and Airflow Using A Rat Whisker. In *2018 7th IEEE International Conference on Biomedical Robotics and Biomechatronics (Biorob)*, pages 1187–1192, August 2018. doi: 10.1109/BIOROB.2018.8487886. ISSN: 2155-1782.

[68] J. Sullivan, Ben Mitchinson, Martin Pearson, Mathew Evans, Nathan Lepora, Charles Fox, Chris Melhuish, and Tony Prescott. Tactile Discrimination Using Active Whisker Sensors. *Sensors Journal, IEEE*, 12:350–362, March 2012. doi: 10.1109/JSEN.2011.2148114.

[69] Kuniharu Takei, Zhibin Yu, Maxwell Zheng, Hiroki Ota, Toshitake Takahashi, and Ali Javey. Highly sensitive electronic whiskers based on patterned carbon nanotube and silver nanoparticle composite films. *Proceedings of the National Academy of Sciences*, 111 (5):1703–1707, February 2014. doi: 10.1073/pnas.1317920111. URL https://www.pnas.org/doi/10.1073/pnas.1317920111. Publisher: Proceedings of the National Academy of Sciences.

[70] Martin Pearson, Anthony Pipe, Chris Melhuish, Ben Mitchinson, and Tony Prescott. Whiskerbot: A Robotic Active Touch System Modeled on the Rat Whisker Sensory System. *Adaptive Behavior - ADAPT BEHAV*, 15:223–240, September 2007. doi: 10.1177/1059712307082089.

[71] Mathew Evans, Charles Fox, Martin Pearson, and Tony Prescott. Spectral template based classification of robotic whisker sensor signals in a floor texture discrimination task. January 2009.

[72] Martin Pearson, Ben Mitchinson, Jason Welsby, Tony Pipe, and Tony Prescott. SCRATCHbot: Active Tactile Sensing in a Whiskered Mobile Robot. pages 93–103, September 2010. ISBN 978-3-642-15192-7. doi: 10.1007/978-3-642-15193-4_9.

[73] Martin Pearson, Ben Mitchinson, J. Sullivan, Anthony Pipe, and Tony Prescott. Biomimetic vibrissal sensing for robots. *Philosophical transactions of the Royal Society of London. Series B, Biological sciences*, 366: 3085–96, November 2011. doi: 10.1098/rstb.2011.0164.

[74] Tareq Assaf, Emma D. Wilson, Sean Anderson, Paul Dean, John Porrill, and Martin J. Pearson. Visual-tactile sensory map calibration of a biomimetic whiskered robot. In *2016 IEEE International Conference on Robotics and Automation (ICRA)*, pages 967–972, May 2016. doi: 10.1109/ICRA.2016.7487228.

[75] Martin Pearson, Ian Gilhespy, Chris Melhuish, Ben Mitchinson, Mokhtar Nibouche, Anthony Pipe, and Tony Prescott. A Biomimetic Haptic Sensor. *International Journal of Advanced Robotic Systems*, 2, December 2005. doi: 10.5772/5774.

[76] Ben Mitchinson, Chris J Martin, Robyn A Grant, and Tony J Prescott. Feedback control in active sensing: rat exploratory whisking is modulated by environmental contact. *Proceedings of the Royal Society B: Biological Sciences*, 274(1613):1035–1041, February 2007. doi: 10.1098/rspb.2006.0347. URL https://royalsocietypublishing.org/doi/10.1098/rspb.2006.0347. Publisher: Royal Society.

[77] Festo Didactic InfoPortal, . URL https://ip.festo-didactic.com/InfoPortal/Robotino3/Overview/EN/index.html.

[78] elumotion.com :: Home, . URL http://elumotion.com/.

[79] Zachary Pezzementi, Erion Plaku, Caitlin Reyda, and Gregory D. Hager. Tactile-Object Recognition From Appearance Information. *IEEE Transactions on Robotics*, 27(3):473–487, June 2011. ISSN 1941-0468. doi: 10.1109/TRO.2011.2125350. Conference Name: IEEE Transactions on Robotics.

[80] D.G. Lowe. Object recognition from local scale-invariant features. In *Proceedings of the Seventh IEEE*

International Conference on Computer Vision, volume 2, pages 1150–1157 vol.2, September 1999. doi: 10.1109/ICCV.1999.790410.

[81] A Statistical Approach to Texture Classification from Single Images | SpringerLink, . URL https://link.springer.com/article/10.1023/B:VISI.0000046589.39864.ee.

[82] Shan Luo, Wenxuan Mou, Kaspar Althoefer, and Hongbin Liu. Novel Tactile-SIFT Descriptor for Object Shape Recognition. *IEEE Sensors Journal*, 15 (9):5001–5009, September 2015. ISSN 1558-1748. doi: 10.1109/JSEN.2015.2432127. Conference Name: IEEE Sensors Journal.

[83] Radu Bogdan Rusu, Zoltan Csaba Marton, Nico Blodow, and Michael Beetz. Learning informative point classes for the acquisition of object model maps. In *Robotics and Vision 2008 10th International Conference on Control, Automation*, pages 643–650, December 2008. doi: 10.1109/ICARCV.2008.4795593.

[84] Gabriela Zarzar Gandler, Carl Henrik Ek, Mårten Björkman, Rustam Stolkin, and Yasemin Bekiroglu. Object shape estimation and modeling, based on sparse Gaussian process implicit surfaces, combining visual data and tactile exploration. *Robotics and Autonomous Systems*, 126:103433, April 2020. ISSN 0921-8890. doi: 10.1016/j.robot.2020.103433. URL https://www.sciencedirect.com/science/article/pii/S0921889019303495.

[85] Anna Petrovskaya and Oussama Khatib. Global Localization of Objects via Touch. *IEEE Transactions on Robotics*, 27(3):569–585, June 2011. ISSN 1941-0468. doi: 10.1109/TRO.2011.2138450. Conference Name: IEEE Transactions on Robotics.

[86] Martin Meier, Matthias Schopfer, Robert Haschke, and Helge Ritter. A Probabilistic Approach to Tactile Shape Reconstruction. *IEEE Transactions on Robotics*, 27(3):630–635, June 2011. ISSN 1941-0468. doi: 10.1109/TRO.2011.2120830. Conference Name: IEEE Transactions on Robotics.

[87] Sudharshan Suresh, Maria Bauza, Kuan-Ting Yu, Joshua G. Mangelson, Alberto Rodriguez, and Michael Kaess. Tactile SLAM: Real-time inference of shape and pose from planar pushing. In *2021 IEEE International Conference on Robotics and Automation (ICRA)*, pages 11322–11328, May 2021. doi: 10.1109/ICRA48506.2021.9562060. ISSN: 2577-087X.

[88] Marcin Szwed, Knarik Bagdasarian, and Ehud Ahissar. Encoding of vibrissal active touch. *Neuron*, 40(3):621–630, October 2003. ISSN 0896-6273. doi: 10.1016/s0896-6273(03)00671-8.

[89] M. Shoykhet, D. Doherty, and D. J. Simons. Coding of deflection velocity and amplitude by whisker primary afferent neurons: implications for higher level processing. *Somatosensory & Motor Research*, 17 (2):171–180, 2000. ISSN 0899-0220. doi: 10.1080/08990220050020580.

[90] Kelly Graham. *Fundamentals of Mechanical Vibration*. McGraw-Hill Inc.,US, February 2000. ISBN 978-0-07-230092-5.

[91] M. Kaneko, N. Kanayama, and T. Tsuji. Active antenna for contact sensing. *IEEE Transactions on Robotics and Automation*, 14(2):278–291, April 1998. ISSN 2374-958X. doi: 10.1109/70.681246. Conference Name: IEEE Transactions on Robotics and Automation.

[92] Christoph Will, Joachim Steigenberger, and Carsten Behn. Object Contour Reconstruction using Bio-inspired Sensors. volume 1, September 2014. doi: 10.5220/0005018004590467.

[93] Joseph H. Solomon and Mitra J. Z. Hartmann. Artificial Whiskers Suitable for Array Implementation: Accounting for Lateral Slip and Surface Friction. *IEEE Transactions on Robotics*, 24(5):1157–1167, October 2008. ISSN 1941-0468. doi: 10.1109/TRO.2008.2002562. Conference Name: IEEE Transactions on Robotics.

[94] Probabilistic robotics. *Communications of the ACM*, 45(3):52–57, March 2002. ISSN 0001-0782, 1557-7317. doi: 10.1145/504729.504754. URL https://dl.acm.org/doi/10.1145/504729.504754.

[95] Lucie Huet, John Rudnicki, and Mitra Hartmann. Tactile Sensing with Whiskers of Various Shapes: Determining the Three-Dimensional Location of Object Contact Based on Mechanical Signals at the Whisker Base. *Soft Robotics*, 4:88–102, June 2017. doi: 10.1089/soro.2016.0028.

[96] Charles R. Qi, Hao Su, Kaichun Mo, and Leonidas J. Guibas. PointNet: Deep Learning on Point Sets for 3D Classification and Segmentation, April 2017. URL http://arxiv.org/abs/1612.00593. arXiv:1612.00593 [cs].

[97] R Andrew Russell and Jaury Adi Wijaya. Object Location and Recognition using Whisker Sensors.

[98] Charles W. Fox and Tony J. Prescott. Mapping with Sparse Local Sensors and Strong Hierarchical Priors. In Roderich Groß, Lyuba Alboul, Chris Melhuish, Mark Witkowski, Tony J.

Prescott, and Jacques Penders, editors, *Towards Autonomous Robotic Systems*, volume 6856, pages 183–194. Springer Berlin Heidelberg, Berlin, Heidelberg, 2011. ISBN 978-3-642-23231-2 978-3-642-23232-9. doi: 10.1007/978-3-642-23232-9_17. URL http://link.springer.com/10.1007/978-3-642-23232-9_17. Series Title: Lecture Notes in Computer Science.

[99] Ying Zhang, Juan Liu, Gabriel Hoffmann, Mark Quilling, Kenneth Payne, Prasanta Bose, and Andrew Zimdars. Real-time indoor mapping for mobile robots with limited sensing. pages 636–641, December 2010. doi: 10.1109/MASS.2010.5663778.

[100] A. Zelinsky, Y. Kuniyoshi, and H. Tsukune. Monitoring and co-ordinating behaviours for purposive robot navigation. In *Proceedings of IEEE/RSJ International Conference on Intelligent Robots and Systems (IROS'94)*, volume 2, pages 894–901 vol.2, September 1994. doi: 10.1109/IROS.1994.407487.

[101] Rolf Pfeifer and Paul Verschure. *Distributed Adaptive Control : A Paradigm for Designing Autonomous Agents.* Technical Report: AI-memo 1991-7., 1991.

[102] Paul F. M. J. Verschure, Ben J. A. Kröse, and Rolf Pfeifer. Distributed adaptive control: The self-organization of structured behavior. *Robotics and Autonomous Systems*, 9(3):181–196, January 1992. ISSN 0921-8890. doi: 10.1016/0921-8890(92)90054-3. URL https://www.sciencedirect.com/science/article/pii/0921889092900543.

[103] Lukas Schmid, Michael Pantic, Raghav Khanna, Lionel Ott, Roland Siegwart, and Juan Nieto. An Efficient Sampling-Based Method for Online Informative Path Planning in Unknown Environments. *IEEE Robotics and Automation Letters*, 5:1–1, January 2020. doi: 10.1109/LRA.2020.2969191.

[104] Gregory Hitz, Enric Galceran, Marie-Ève Garneau, François Pomerleau, and Roland Siegwart. Adaptive continuous-space informative path planning for online environmental monitoring. *Journal of Field Robotics*, 34(8):1427–1449, 2017. ISSN 1556-4967. doi: 10.1002/rob.21722. URL https://onlinelibrary.wiley.com/doi/abs/10.1002/rob.21722. _eprint: https://onlinelibrary.wiley.com/doi/pdf/10.1002/rob.21722.

[105] Ting Zhang, Tian Zhou, Bradley S. Duerstock, and Juan P. Wachs. Image Exploration Procedure Classification with Spike-timing Neural Network for the Blind. In *2018 24th International Conference on Pattern Recognition (ICPR)*, pages 3256–3261, August 2018. doi: 10.1109/ICPR.2018.8545312. ISSN: 1051-4651.

[106] T. Bailey and H. Durrant-Whyte. Simultaneous localization and mapping (SLAM): part II. *IEEE Robotics & Automation Magazine*, 13(3):108–117, September 2006. ISSN 1558-223X. doi: 10.1109/MRA.2006.1678144. Conference Name: IEEE Robotics & Automation Magazine.

[107] Hugh Durrant-Whyte and Tim Bailey. Simultaneous Localisation and Mapping (SLAM): Part I The Essential Algorithms. page 9.

[108] Feryal M. P. Behbahani, Ruth Taunton, Andreas A. C. Thomik, and A. Aldo Faisal. Haptic SLAM for context-aware robotic hand prosthetics - simultaneous inference of hand pose and object shape using particle filters. In *2015 7th International IEEE/EMBS Conference on Neural Engineering (NER)*, pages 719–722, April 2015. doi: 10.1109/NER.2015.7146724. ISSN: 1948-3554.

[109] Ben Mitchinson, Martin Pearson, Anthony Pipe, and Tony Prescott. The Emergence of Action Sequences from Spatial Attention: Insight from Rodent-Like Robots. July 2012. ISBN 978-3-642-31524-4. doi: 10.1007/978-3-642-31525-1_15.

[110] Mathew Evans, Charles Fox, Martin Pearson, and Tony Prescott. Tactile Discrimination Using Template Classifiers: Towards a Model of Feature Extraction in Mammalian Vibrissal Systems. pages 178–187, August 2010. ISBN 978-3-642-15192-7. doi: 10.1007/978-3-642-15193-4_17.

[111] R. J. Sinclair, J. J. Kuo, and H. Burton. Effects on discrimination performance of selective attention to tactile features. *Somatosensory & Motor Research*, 17 (2):145–157, 2000. ISSN 0899-0220. doi: 10.1080/08990220050020562.

[112] S. Stansfield. Primitives, features, and exploratory procedures: Building a robot tactile perception system. In *1986 IEEE International Conference on Robotics and Automation Proceedings*, volume 3, pages 1274–1279, April 1986. doi: 10.1109/ROBOT.1986.1087541.

[113] David Ball, Scott Heath, Janet Wiles, Gordon Wyeth, Peter Corke, and Michael Milford. OpenRatSLAM: an open source brain-based SLAM system. *Autonomous Robots*, 34:1–28, April 2013. doi: 10.1007/s10514-012-9317-9.

[114] Yan S. W. Yu, Matthew M. Graff, and Mitra J. Z. Hartmann. Mechanical responses of rat vibrissae to airflow. *Journal of Experimental Biology*, 219(7):937–948, April 2016. ISSN 0022-0949. doi: 10.1242/

jeb.126896. URL https://doi.org/10.1242/jeb.126896.

[115] Roomba® Robot Vacuum Cleaners | iRobot®, . URL https://www.irobot.com/en_US/roomba.html.

[116] Shiyao Huang and Hao Wu. Texture Recognition Based on Perception Data from a Bionic Tactile Sensor. *Sensors*, 21:5224, August 2021. doi: 10.3390/s21155224.

[117] Christopher M. Bishop, Geoffrey Hinton, Christopher M. Bishop, and Geoffrey Hinton. *Neural Networks for Pattern Recognition*. Oxford University Press, Oxford, New York, November 1995. ISBN 978-0-19-853864-6.

[118] Ben Mitchinson, Kevin N. Gurney, Peter Redgrave, Chris Melhuish, Anthony G. Pipe, Martin Pearson, Ian Gilhespy, and Tony J. Prescott. Empirically inspired simulated electro-mechanical model of the rat mystacial follicle-sinus complex. *Proceedings of the Royal Society B: Biological Sciences*, 271(1556):2509–2516, December 2004. ISSN 0962-8452. doi: 10.1098/rspb.2004.2882. URL https://www.ncbi.nlm.nih.gov/pmc/articles/PMC1691889/.

[119] Susanne Sterbing-D'Angelo, Mohit Chadha, Chen Chiu, Benjamin Falk, Wei Xian, Janna Barcelo, John Zook, and Cynthia Moss. Bat wing sensors support flight control. *Proceedings of the National Academy of Sciences of the United States of America*, 108:11291–6, June 2011. doi: 10.1073/pnas.1018740108.

[120] A.M.K. Dagamseh, C.M. Bruinink, H. Droogendijk, R.J. Wiegerink, T.S.J. Lammerink, and G.J.M. Krijnen. Engineering of biomimetic hair-flow sensor arrays dedicated to high-resolution flow field measurements. In *2010 IEEE SENSORS*, pages 2251–2254, November 2010. doi: 10.1109/ICSENS.2010.5690705. ISSN: 1930-0395.

[121] A.M.K. Dagamseh, T.S.J. Lammerink, R. Sanders, R.J. Wiegerink, and G.J.M. Krijnen. Towards high-resolution flow cameras made of artificial hair flow-sensors for flow pattern recognition. In *2011 IEEE 24th International Conference on Micro Electro Mechanical Systems*, pages 648–651, January 2011. doi: 10.1109/MEMSYS.2011.5734508. ISSN: 1084-6999.

[122] Matthew Maschmann, Gregory Ehlert, Benjamin Dickinson, David Phillips, Cody Ray, Greg Reich, and Jeff Baur. Bioinspired Carbon Nanotube Fuzzy Fiber Hair Sensor for Air-Flow Detection. *Advanced materials (Deerfield Beach, Fla.)*, 26, May 2014. doi: 10.1002/adma.201305285.

[123] Avner Wallach, Knarik Bagdasarian, and Ehud Ahissar. On-going computation of whisking phase by mechanoreceptors. *Nature Neuroscience*, 19(3):487–493, March 2016. ISSN 1546-1726. doi: 10.1038/nn.4221. URL https://www.nature.com/articles/nn.4221. Number: 3 Publisher: Nature Publishing Group.

[124] Kyle S. Severson, Duo Xu, Margaret Van de Loo, Ling Bai, David D. Ginty, and Daniel H. O'Connor. Active Touch and Self-Motion Encoding by Merkel Cell-Associated Afferents. *Neuron*, 94(3):666–676.e9, May 2017. ISSN 0896-6273. doi: 10.1016/j.neuron.2017.03.045. URL https://www.sciencedirect.com/science/article/pii/S0896627317302891.

[125] SpeedyBee FS225 V2 5 inch Frame, . URL https://www.speedybee.com/speedybee-fs225-v2-5-inch-frame/.

[126] mRo PixRacer R15, . URL https://store.mrobotics.io/product-p/auav-pxrcr-r15-mr.htm.

[This page is intentionally left blank]

Part IV

References

*References cited in Introduction of report.

[This page is intentionally left blank]

References

[1] D. Jung et al. “Whisker based mobile robot navigation”. In: *Proceedings of IEEE/RSJ International Conference on Intelligent Robots and Systems. IROS ’96*. Vol. 2. Nov. 1996, 497–504 vol.2. DOI: 10.1109/IROS.1996.570842.

[2] Yulai Zhang et al. “A Small-Scale, Rat-Inspired Whisker Sensor for the Perception of a Biomimetic Robot: Design, Fabrication, Modeling, and Experimental Characterization”. In: *IEEE Robotics & Automation Magazine* 29.4 (Dec. 2022). Conference Name: IEEE Robotics & Automation Magazine, pp. 115–126. DOI: 10.1109/MRA.2022.3182870.

[3] Chenxi Xiao et al. “Active Multiobject Exploration and Recognition via Tactile Whiskers”. In: *IEEE Transactions on Robotics* 38.6 (Dec. 2022). Conference Name: IEEE Transactions on Robotics, pp. 3479–3497. DOI: 10.1109/TRO.2022.3182487.

[This page is intentionally left blank]

Part V

Appendices

[This page is intentionally left blank]

A

System Architecture

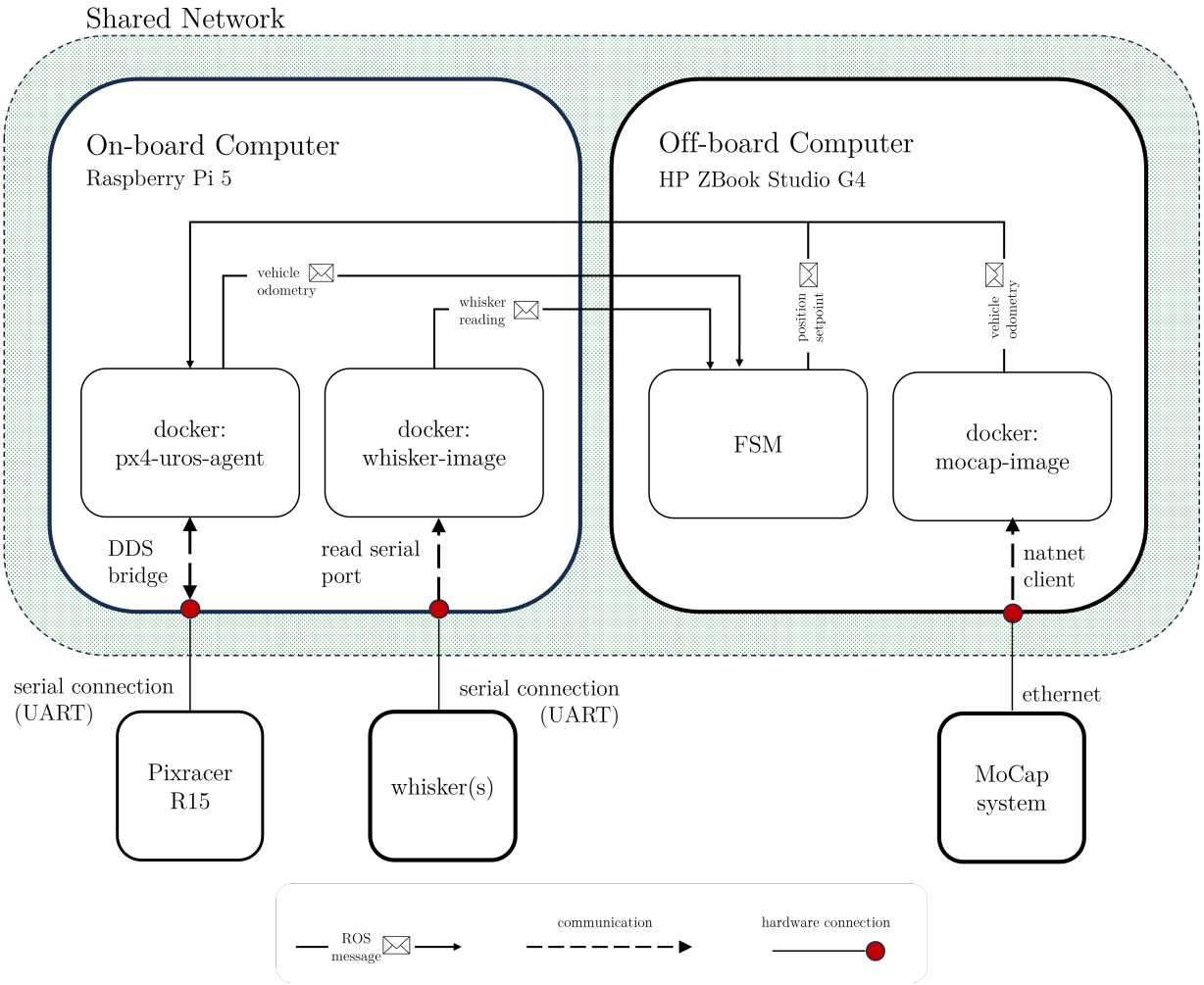

Figure A.1: System architecture

[This page is intentionally left blank]

B

PX4 Position Controller

As discussed in the paper, the research involved feeding trajectory set-points to the PX4 controller. During testing, it became evident that the position control was unable to achieve precise tracking. The primary issues were that the controller failed to respond effectively to sudden changes in set-points and showed inadequate response when set-points were too small. This behavior is particularly problematic when operating in close proximity to obstacles. After consulting forums, it was discovered that the best tracking others had managed was within a 0.05m margin of the set-point. Although completely resolving the issue was unlikely, several attempts were made to optimize the controller's performance. Below are the approaches that were tested:

1. **PID Tuning:** Efforts were made to tune the position (P) and velocity (PID) controllers. Increasing the P gains slightly improved response and reduced significant errors, particularly when holding position. However, these adjustments did not enhance the contour following performancethe PX4 controller still failed to respond adequately to sudden or large inputs. Modifying the I gain had no noticeable effect, and altering the D gain led to instability.
2. **Feed-Forward Velocity:** To specifically improve wall-following performance, feed-forward velocity set-points were calculated alongside the trajectory set-points and fed into the PX4 controller. This approach aimed to circumvent the position controller's sluggish response by directly providing a feed-forward velocity term to the velocity controller. Although this method showed promise, time constraints prevented optimization. Issues arose, such as increased velocity set-points requiring greater acceleration, leading to more aggressive collisions with the wall. Additionally, sudden accelerations distorted the whisker signals.
3. **EMA Filtering:** The final approach involved applying an Exponential Moving Average (EMA) filter. Rather than attempting to force the controller to work with the given inputs, the inputs were adjusted to better suit the controller's capabilities. The filter was used to smooth the controller's inputs; however, over-smoothing could slow the system's response, increasing the risk of collisions. After testing various window sizes, a window of N=20 was selected as the optimal compromise.